NUREG/CR-3527
LA-9913-MS

RD

Material Transport Analysis for Accident-Induced Flow in Nuclear Facilities

R. A. Martin
P. K. Tang
A. P. Harper
J. D. Novat
W. S. Gregory

Manuscript submitted: September 1983
Date published: October 1983

Prepared for
Division of Risk Analysis
Office of Nuclear Regulatory Research
US Nuclear Regulatory Commission
Washington, DC 20555

NRC FIN No. A7029

Los Alamos National Laboratory
Los Alamos, New Mexico 87545

CONTENTS

MATERIAL TRANSPORT ANALYSIS FOR ACCIDENT-INDUCED FLOW IN NUCLEAR FACILITIES

by

R. A. Martin, P. K. Tang, A. P. Harper,
J. D. Novat, and W. S. Gregory

ABSTRACT

This report is a summary of the material transport modeling procedures developed to support a family of accident analysis computer codes. The material transport modeling areas include transport initiation, convection, interaction, depletion, and filtration. Except for material interaction, these areas are developed in modular form in three Los Alamos National Laboratory computer codes: TORAC, EXPAC, and FIRAC. This family of codes was developed to provide improved methods of tornado, explosion, and fire accident consequence assessment, respectively, for the nuclear industry. Although the codes were designed to estimate accident-induced gas-dynamic, thermal, and material transport transient phenomena in nuclear fuel cycle facility ventilation systems, they are applicable to other facilities as well. Sample problems using TORAC have been provided to illustrate the current material transport capabilities for a simple system under tornado-induced accident conditions. Some suggestions for future improvements to some of these material transport models also are discussed.

I. INTRODUCTION

Nuclear facilities must be designed to protect the general public from the consequences of accidents that could result in a release of radioactive material to the environment. To ensure that nuclear facilities can withstand postulated accidents, regulatory agencies are responsible for reviewing proposed facility designs. The degree of conservatism and the related risk assessment also must

be evaluated for these accident conditions. The nature of the hazardous material involved and the potential for accidents require that designers and analysts have methods and supportive experimental data for a systematic approach to estimating accident effects.

Assessment of the environmental consequences of an accident ultimately involves calculating the atmospheric dispersion of radioactive materials and estimating the radiation dose to the surrounding population. Some uncertainty lies in the estimate of the nuclear facility source term to be used for atmospheric dispersion calculations. In current safety analyses, some conservative assumptions are used to assess worst cases. Such assumptions are made to insure that the consequences are not underestimated. The current program is intended to improve our ability to more accurately estimate nuclear facility source terms. Thus, we have undertaken a fuel cycle facility safety analysis program to provide user-oriented tools for making better estimates of accident-induced release or source-term characteristics at a nuclear facility's atmospheric boundary.[1,2] These tools are intended to be an improvement over current safety analysis review techniques. The scope of the program is limited to only accident-induced material movement within a nuclear facility.

The types of plants considered in this study include fuel fabrication, fuel reprocessing, waste solidification, fuel storage, and UF_6 production facilities. However, the planned research work will be applicable to a large spectrum of facility designs and processes. The results will apply to current as well as anticipated Nuclear Regulatory Commission (NRC) licensing and decommissioning actions.

The types of accidents considered in this study include fires, explosions, spills, equipment failures, criticalities, and tornados. The highest priority will be placed on the analysis of fire hazards. These accidents were specified by the NRC Research Review Group (RRG) responsible for technical review of this program.

The fuel cycle safety analysis program is divided into three major research areas.[1] The first area is defining accidents that could occur and defining where and how they could occur inside a given facility. This area includes a description of the facility, its processes or unit operations, process material inventories, safety systems, and transport pathways. The second area is defining the accident energetics and material release relatively close to the accident. Each accident considered will be modeled to describe its near-field

effects. The last area is modeling the gas and material fluxes through the transport pathways up to a containment system or to the atmospheric boundary.

Battelle Pacific Northwest Laboratory (PNL) and Oak Ridge National Laboratory (ORNL) share responsibility for the first and second research areas; our responsibility is the third area. Work in the first two research areas will be to identify the accidents to be considered and also to provide primary source-term data to be used in the transport models. The Los Alamos National Laboratory investigation will include developing techniques for estimating accident-induced transport of material to the nuclear facility's atmospheric boundaries. The Laboratory's objective in this program is to develop mathematical models and experimental data that will permit prediction of material transport through a complex network of rooms, gloveboxes, ductwork, filtration systems, and other components commonly found in ventilation systems. These models will require predicting the accident-induced flow dynamics with special emphasis on the transport of radioactive material.

Work at Los Alamos in the early stages of this project has resulted in a family of accident analysis computer codes (TORAC, EXPAC, and FIRAC). TORAC[3] is a computer code that can predict tornado-induced flows, pressures, and material transport within structures. EXPAC[4] can predict explosion-induced gas-dynamic transients and material transport within structures. FIRAC[5] is designed to predict the simultaneous gas-dynamic, material transport, and thermal transients that occur in a facility subjected to a fire. TVENT[6] and EVENT[7] are the predecessors of these codes. These codes are directed toward nuclear fuel cycle facilities and the primary release pathway—the ventilation system. However, they are applicable to other structures and can be used to model other airflow pathways within a facility.

The objective of this report is to present the material transport modeling procedures developed to support the Los Alamos family of fuel cycle safety analysis computer codes. The material transport modeling areas include transport initiation, convection, interaction, depletion, and filtration. Except for material interaction, these areas are developed in modular form in TORAC, EXPAC, and FIRAC.

The material transport algorithms in our codes provide an estimate of the aerosol or gas transport within a nuclear fuel cycle facility. Ultimately, we would like to predict the quantity and physical and chemical characteristics of radioactive material that may be released from the facility as a result of an

accident. The transport can take place because of airflow through the rooms, cells, canyons, corridors, gloveboxes, and ductwork installed in the facility. In many cases, the entire flow pathway forms a complex network system. Using the computer codes, we can calculate material concentrations and material mass flow rates at any location in the network, including the supply and exhaust ducts of the network system. Most importantly, the codes will perform transport calculations as a function of time for arbitrary user-specified accident transients imposed on the facility boundaries. Although our codes can be used to determine material transport under steady flow conditions if desired, there is no need to assume steady flow as is required in some material transport codes.

In Ref. 8, the material transport estimate is obtained in piecemeal fashion using steady flow calculations for rooms and duct segments. Our codes model the entire network for transient flow and in doing so take into account system interactions. A generalized treatment of material transport under accident conditions could become very complex.[9-15] Several different types of materials could be transported, and more than one phase could be involved, including solids, liquids, and gases with phase transitions. Chemical reactions leading to the formation of new species could occur during transport. Furthermore, there will be a size distribution function that varies with time and position for each type of material, depending on the relative importance of effects such as homogeneous nucleation, coagulation (material interaction), diffusion (both by Brownian motion and by turbulence), and gravitational sedimentation.[9-11] We know of no computer code that can handle transient-flow-induced material transport in a network system subjected to possibly all of these complications, and the transport portion of our codes does not include this level of generality. This initial, basic form of our material transport modeling consists of the following.

- Gas dynamics decoupled from material transport
- Homogeneous mixture and dynamic equilibrium
- Material transport limited to a single size and species (except for FIRAC)
- No material interaction during transport
- Material deposition based on gravitational settling using relationships from the literature
- Turbulent and Brownian diffusion and phoretic effects neglected
- Phase change, chemical reaction, and electrical migration not allowed

- Material entrainment can be arbitrarily specified using tabular inputs or calculated using semi-empirical relationships based on wind tunnel data

Although the material transport capability is limited in these codes, this initial version does represent a significant advance for the prediction of material movement within a nuclear facility. The codes are structured in a modular fashion so that improved modules can be incorporated easily, and this is discussed in Sec. II. Detailed descriptions of the material transport modules now available within the codes and suggested improvements that can reduce the degree of conservatism in our current capabilities are included.

II. MODULAR STRUCTURE

The movement of material by a flowing fluid involves several basic mechanisms. The primary mechanism for movement is the flow of the fluid itself; the other mechanisms involve physical models that could be upgraded as the state of the art improves. The basic elements of material transport that we will consider in an accident-induced flow environment are listed below.

1. Material characteristics
2. Transport initiation
3. Convective transport
4. Transport interaction
5. Aerosol depletion
6. Filtration

Material characteristics and transport initiation are areas that must be considered by the user as he begins to set up a code to solve a given problem. Calculations of convective transport, aerosol depletion, and filtration are performed automatically by the code. Items 2—6 are actually separate subroutines or modules within the code. Item 3 is a key subroutine that calls on items 2, 4, 5, and 6 as needed during the course of the calculation. Each of the components listed above is subject to certain limitations and assumptions that will be discussed below. We also will specify the required user inputs and provide appropriate references for the theory used in each case.

The material transport capability is composed of separate subroutines or modules that can be added or removed without disturbing other parts of the computer codes (Fig. 1). The purpose of this structure is to allow us to begin

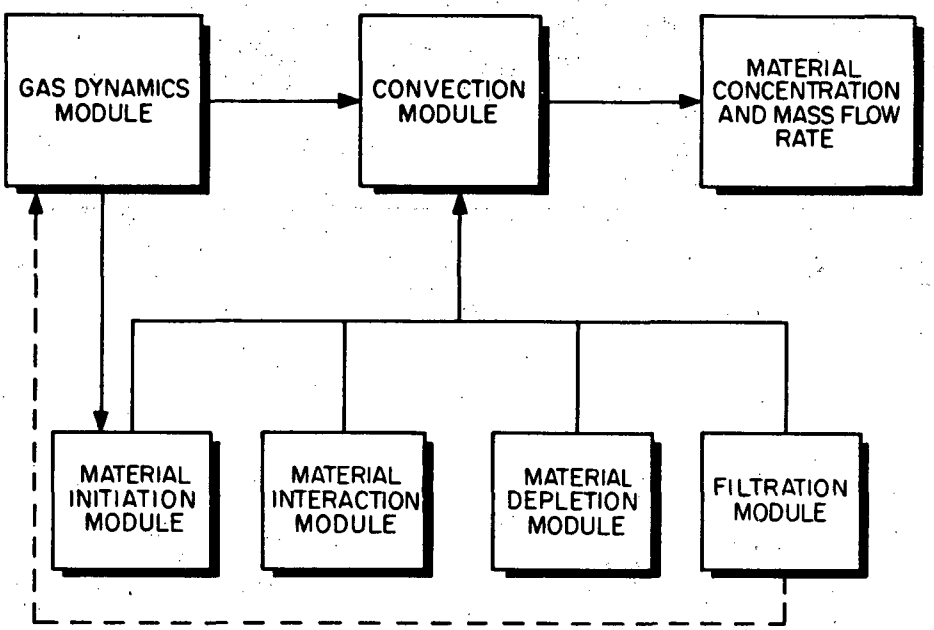

Fig. 1.
Material transport modular structure.

with basic material transport modules based on relationships discussed in the literature. From this initial analysis level[1] we can improve each module so that a more advanced analysis capability can be achieved. When the module is complete, we can simply exchange a new module for an old one without disturbing the rest of the code. With this in mind, we will discuss a number of planned or possible improvements to our material transport modules in the sections that follow, starting with user-supplied material characteristics.

III. MATERIAL CHARACTERISTICS

A. Existing Capability

The limitations on material transport in terms of the physical and chemical characteristics of the material are as follows. For TORAC and EXPAC, the pneumatically transportable contaminant material is restricted to a single phase of a single species. In FIRAC, the contaminant material can consist of any number of aerosol or gaseous species. Thus, multiple-species size distributions can be simulated in FIRAC. However, no coagulation, phase transitions, or chemical reactions are allowed in any of the three codes; for example, condensation and gas-to-particle conversion are not permitted. If the contaminant is an

aerosol (solid particles or liquid droplets suspended in air), then it will be treated in TORAC and EXPAC as monodisperse (equal-sized) and homogeneous (uniform density) and with spherical particles or droplets during a given code run. Both size and density must be specified by the user. If the contaminant is a gas, it is assumed to be inert. User guidance in the area of aerosol and gas characteristics is provided below. Some suggestions also are made for describing fuel-grade plutonium and uranium oxide powders.

In applying the material transport capability in our codes, the user must identify the type (aerosol or gas), quantity, and location of material at risk. If the material is a solid or liquid aerosol, a characteristic size and density must be specified. In the simplest case, these parameters may be assumed. For example, if the user is primarily concerned with the transport of aerosols in the size range of $D_p \leq 12$ μm and densities of $0.5 \leq \rho_p \leq 12$ g/cm^3, he could run a code for some assumed cases of (D_p, ρ_p) to determine entrainment or deposition sensitivity.

In general, the user may wish to characterize a nonideal aerosol contaminant with approximate or idealized values of (D_p, ρ_p). We advise caution here because there are many different ways to characterize the diameter of aerosols of irregular shape and nonuniform density. For example, diameters representing a mean value relative to total count, surface area, volume, weight, or terminal settling velocity can be estimated based on frequency-of-occurrence data.[9-11,16]

For the case of aerosol transport along fuel cycle facility pathways, we are interested in changes in aerosol concentration resulting from entrainment, dilution, deposition, and filtration. Entrainment, deposition, and filtration all depend on the quasi-steady aerodynamic drag characteristics of the aerosol.[9-11] Unless the aerosol is very small (less than 0.5 μm), the probability that a spherical particle or droplet will deposit depends on the magnitude of its terminal settling velocity, u_s.[10]

$$u_s = \rho_p D_p^2 C g / 18\mu \quad , \tag{1}$$

where ρ_p = actual density,
D_p = diameter,
C = Cunningham slip factor,
g = gravitational acceleration, and
μ = aerodynamic viscosity.

Most aerosols (spherical or nonspherical) having the same settling velocity will be distributed throughout a ventilation system network in a similar manner. The recommended deposition parameter is the aerodynamic diameter or Stokes diameter.[10]

(1) The aerodynamic diameter D_a is the diameter of a sphere of unit density having the same terminal speed as the contaminant.

(2) The Stokes diameter D_s is the diameter of a sphere with the same bulk density and terminal speed as the contaminant.

These diameters are related by the equation

$$u_s = \rho_p D_s^2 C_s g/18\mu = \rho_o D_a^2 C_a g/18\mu \quad , \tag{2}$$

where C_s and C_a are the slip factors associated with D_s and D_a, respectively, and ρ_o is the unit density. For the contaminant of interest, D_s or D_a may have been measured directly using such aerodynamic classification devices as impactors, centrifuges, sedimentometers, or air elutriators. (These devices are suitable for measuring the size of irregularly shaped particles.) If possible, an aerodynamic diameter measurement should be based on activity. Otherwise, we recommend using D_a based on mass measurements.

If count-frequency data (for example, based on projected area diameter for irregularly shaped particles) are available for the contaminant, they must be converted to aerodynamic diameter. Such data should be plotted on log-probability paper and fit with a straight line. If this straight-line fit to the data is acceptable, the size distribution is approximately log-normally distributed and may be described completely by two parameters, geometric count median diameter D_{gc} and geometric standard deviation σ_g. Most fine particle systems formed by comminution of a bulk material or grown by accretion have log-normal size distributions, and so this assumption is recommended.[9-11,16]

The user can obtain D_{gc} and σ_g from log-normally distributed count-frequency data. The Hatch-Choate transformation equations now apply. These equations relate D_{gc} and σ_g to a number of other median and mean diameters that may be important, depending on how the toxic substance or activity is related to the physical properties of the particle. For example, the activity may be proportional to the total number, total surface area, or total mass of the particles. We chose to work on a mass basis. The user may calculate the geometric mass median diameter D_{gm}, the volume mean diameter D_v, and the weight mean diameter D_w from[16]

$$\log D_{gm} = \log D_{gc} + 6.908 \log^2 \sigma_g \quad ,$$

$$\log D_v = \log D_{gc} + 3.454 \log^2 \sigma_g \quad , \text{ and} \qquad (3)$$

$$\log D_w = \log D_{gc} + 8.023 \log^2 \sigma_g \quad ,$$

where the logarithms are calculated using base 10. The median diameters D_{gc} and D_{gm} referred to above divide the count-based and mass-based size distributions in half. For example, half of the mass of the sample lies above D_{gm} and half below. A mean diameter is the diameter of a hypothetical particle that is intended to represent the total number of particles in the sample.

In the absence of specific information on the aerodynamic properties of the aerosol of interest, Stockham[16] recommends using D_w as an approximation of aerodynamic size. An alternative is to convert D_v to an aerodynamic diameter. (If we assume the material density to be uniform, independent of size, and known, then the mass of the particle with size D_v is a mean mass.) To do this use

$$D_a = \left[(6/\pi)(\rho_p/\rho_o)(\alpha_3/K_r)\right]^{1/2} D_v \quad , \qquad (4)$$

where α_3 = volume shape factor and
K_r = resistance shape factor.[10]

The values of α_3 and K_r are given in Ref. 10, where this calculation is discussed.

We advise caution in estimating aerosol density. The aerosol produced by accident conditions may in fact consist of flocculi and agglomerates with actual densities well below the theoretical density of the pure parent materials. The floc densities may be as much as an order of magnitude less than the normal density.[16] The user can find pertinent information on fuel-grade powder size and density in Refs. 2 and 17—30. Useful information on droplet sizes and densities can be found in Ref. 2.

B. Future Improvements

We are interested in removing some of the idealizations discussed in Sec. III.A. that impose limitations on our ability to model the transport of real materials of concern in fuel cycle facilities. In particular, the multiple species capability currently available in FIRAC[5] should be extended to TORAC[3] and EXPAC.[4] This improvement (going from single to multiple species capability) forms the foundation for transient calculations of the time- and space-dependent material size-distribution function. Here a multiple-species capability encompasses the ability to model a set of contiguous size intervals representing the discrete size distribution function of a single species. Estimates of aerosol mass exchange between intervals of the size distribution function then depend on the validity of our physical models for aerosol production (gas-to-particle conversion, entrainment, or other mechanism), interaction, and depletion.

Given the capability of modeling aerosol size distribution functions, a significant improvement for the user would be a built-in calculation of the log-normal size distribution function. This distribution is particularly useful in particle size analysis because it is easy to manipulate mathematically and experimental observations show that it fits a wide variety of aerosol populations. Assuming a log-normal distribution for a given aerosol species, the relative number of particles or droplets having diameters whose logarithms fall in the interval $x \pm dx/2$ is given by

$$f(x)dx = \frac{1}{\sqrt{2\pi}\,\sigma} \exp\left[-\left[(x - \mu_0)^2/2\sigma^2\right]\right] dx \quad ,$$

where $x = \ln D$,

$\sigma = \ln \sigma_g$,

$\mu_o = \ln D_{gc}$, and

$f(x)$ = log-normal probability density function.

"ln" implies logarithms to base "e". With these expressions and knowing the total aerosol mass together with ρ_p, D_{gc} (or D_{gm}), and σ_g specified by the user, our codes could partition the available mass over n increments, such as between log sizes $\pm 3\ \sigma_g$. This code-calculated distribution of each aerosol would be a convenient starting point for transient calculations.

IV. TRANSPORT INITIATION

A. Background

To calculate material transport, the analyst must determine or assume the location, distribution, and total quantity of contaminant material. The contaminant may be located in any or all rooms, cells, gloveboxes, corridors, or rectangular ducts. (An assumption about material distribution is only necessary when the user wishes to exercise the "calculated aerodynamic entrainment of dry powder from thick beds" option discussed below.) A total quantity (mass of material) must be known or assumed.

There are two options for material transport initiation, and they can be used simultaneously. These are user-specified and calculated aerodynamic entrainment. The user-specified option gives the analyst considerable flexibility but requires engineering judgment to specify input to the code. This option involves preparing a table or graph of material generation rate or mass injection rate (kilograms per second vs time). The data are supplied to the code on the input deck Material Generation Cards. For example, a given cell can have a given quantity of fuel-grade uranium or plutonium powder injected at a specified rate; the injected material also could be a gas. This user-specified option may be selected to calculate the consequences of a hypothetical aerosol or gaseous release, and for reasons discussed below, we recommend using it to handle reentrainment from thin beds (dirty cells or ductwork). Our codes have been developed assuming that accident-induced off-design flows are the primary cause of source-term initiation. A general-purpose utility code may be used for

accidents that do not significantly disrupt the normal ventilation system flow, such as pressurized releases (if not too severe), spills, and equipment failures. Guidance for user source-term estimation can be found below.

The user may wish to specify a material generation rate vs time for many accidents. This procedure is the same as that discussed above; that is, a table or graph of mass injection rates can be specified to simulate the injection of material associated with the accident.

The calculated entrainment option refers specifically to a subroutine designed to calculate aerodynamic entrainment of dry powder from thick beds. This subroutine can be useful for analysis of flow-induced material transport initiation. It uses a new semi-empirical analytical approach that takes advantage of detailed flow information produced by the gas-dynamics module for calculating entrainment. To arrive at an estimate of the mass of material entrained at each time step of calculation, this subroutine calculates when the surface particles will begin to move. Particle, surface, and flow characteristics are taken into account to do this. It also accounts for the aerodynamic, interparticle (cohesion), and surface-to-particle (adhesion) forces that may be acting. This procedure was used previously in Ref. 31 and is discussed more fully there and below.

The user may use this calculated entrainment option whenever powder beds are known or assumed to be present in rooms, cells, gloveboxes, corridors, or rectangular ducts. He must provide the code with particle size and density, total mass of contaminant, and the width and length of the (assumed floor) surface over which the powder is uniformly distributed. If material transport is requested, the user must select at least one of the material transport initiation options. Both options may be used simultaneously.

B. Existing Capability

Our accident analysis computer codes provide the analyst with two options for transport initiation: (1) user specification of mass injection rate vs time and (2) calculated aerodynamic entrainment. These options are quite different and require different levels of effort and judgment from the analyst. In this section we will provide background information to help the user supply numbers for source-term initiation using option (1). We will describe in detail the procedure and equations used with option (2). The primary cause of initiation is assumed to be transient flow induced by an accident. Two examples illustrating the use of option (1) will be discussed first.

As a first example, consider a decomissioned fuel reprocessing facility with contaminated enclosures. The analyst can estimate the preaccident aerosol concentrations in these areas using the resuspension factor concept.[2,17,32-34] The resuspension factor K has been used extensively to quantify airborne contamination levels in operational fuel cycle facilities. By definition,

$$K = \frac{\text{aerosol concentration } (g/m^3)}{\text{surface loading } (g/m^2)} \quad , 1/m \quad .$$

Sutter[17] has tabulated ranges of K that were compiled from numerous references. Her tables include values of K derived from measurements of airborne contamination resulting from numerous and varied cases of outdoor wind stresses and indoor mechanical stresses. Sutter's summary tables are useful for obtaining bracketing or bounding values of K. With assumed or measured values of K and surface loading, the user can calculate the airborne material concentration subject to transport. Based on the enclosure volume, a quantity or mass of contaminant subject to transport can be calculated from the concentration. This mass then can be injected at the system node representing the enclosure of interest using the user-specified option. The mass injection rate must be specified by the user.

Healy[32] reviewed many measurements and applications of this simplistic resuspension factor concept. Several of its limitations are noteworthy. First, the measured values of K range over 11 orders of magnitude. For benign conditions where K is most reliable, the uncertainty is at least 2 orders of magnitude. Further, K fails to account for particle, surface, or local flow characteristics except as they existed during a particular measurement. Thus, we recommend using the resuspension factor only for estimating preaccident airborne mass subject to transport as suggested by this example.

As a second example, consider a mixed-oxide fuel fabrication facility in which bulk MOX or "mixed oxide" powder is being protected. The user may elect to model this facility and run the code for an accident transient without material transport. This preliminary run would supply an estimate of the system gas-dynamic transients, including flow rates and pressure drops during the accident. Some controlled areas may be subjected to abnormally high air

velocities that could lead to entrainment because of aerodynamic stress. A knowledge of the air velocity time history will be useful to estimate the quantity of material made airborne.

We will summarize briefly three methods that can be used to estimate aerodynamic entrainment of aerosol material. Sutter[17] has reviewed and compiled data from numerous papers under the heading "aerodynamic entrainment." (This paper is a good source of reference information.) The analyst's objective here should be to estimate a quantity of material made airborne during the first part of or during the entire accident transient. This quantity then must be converted to a mass injection rate for input to a code as in the first example.

The first method for estimating the quantity of material made airborne by aerodynamic entrainment is to use the "per cent airborne" and "resuspension flux" data measured by Mishima and Schwendiman.[30] As an example, they measured entrainment of uranium dioxide powder and uranium nitrate solution at different air velocities. (Using these data will require using engineering judgment.) A second method for estimating entrainment is to use the results developed by Singer et al.[35,36] to estimate coal dust entrainment. These results also are discussed by Sutter.[17]

Finally, the analyst may use the resuspension rate concept introduced by Sehmel.[37] Resuspension rate is defined as a fraction of the initial mass resuspended per second. By definition,

$$S = \frac{A}{G\Delta t} ,$$

where S = resuspension rate, fraction/s,
A = mass suspended and flowing horizontally through a given cross-sectional area, g,
G = ground source mass, g, and
Δt = duration of sampling, s.

Measurements of S obtained during a number of atmospheric field tests are tabulated in Sutter's paper.[17] The user should become familiar with the limitations of all three of the above methods so that he can apply them judiciously.

Here we will present in detail the procedure and equations used with option (2), calculated aerodynamic entrainment of dry powder from thick beds. The entrainment subroutine has the advantage of calculating entrainment automatically. As with the three methods discussed in the second example above, our objective is to provide the material convection module with an estimate of the quantity of particulate material that can be entrained from a contaminated surface as a result of accident-induced transient flow conditions. However, the previous three methods are not suitable for use in a computer code because they are based on steady-state measurements for specific conditions. Except for Singer's[35] work with coal dust, they fail to couple unsteady flow (changing velocity) conditions to the amount of material entrained. In addition to local flow characteristics, the previous methods do not account for material or surface characteristics in a systematic way. Thus, resuspension factor, resuspension rate, and per cent airborne would have to be measured for innumerable cases to encompass accident conditions.

The analytical method used in our codes for calculating aerodynamic entrainment was proposed and illustrated in a fuel cycle facility application in Ref. 31. To estimate the quantity of material entrained, this method considers the following questions. (1) When does the surface material begin to move? (2) What criterion determines when material will be suspended? (3) How much material becomes suspended? A valid answer to question (1) implies that particle, surface, and flow characteristics have been taken into account. Some account also must be taken of the forces present, namely, aerodynamic, interparticle (cohesion), and surface to particle (adhesion) forces. This procedure is similar to the approach taken by Travis,[38] who developed a computer model to predict reentrainment and redistribution of soil contaminants as a result of eolian effects.

The first question we must answer is "When does material begin to move?" Before particle motion can occur, a threshold airspeed must be equalled or exceeded so that the aerodynamic forces will be sufficient to overcome restraining forces. To relate threshold airspeed to surface effects, we introduce the friction speed equation,

$$u_* = \sqrt{\tau / \rho} \quad , \tag{5}$$

where τ = mean shear stress at the surface and
ρ = fluid density.

Experimental measurements of threshold friction speed u_{*t} obtained at the onset of material movement are available for a wide range of material sizes and densities.

These measurements were plotted in Fig. 2 (from Ref. 39) and are fitted by the following semi-empirical equations.[40]

$$A = \left(0.108 + 0.0323/B - 0.00173/B^2\right) \times \left(1 + 0.055\ /\rho_p g\ D_p^2\right)^{1/2} , \tag{6a}$$

where $A = u_{*t}/\left[(\rho_p - \rho)\, gD_p/\rho\right]^{1/2}$,
$B = u_{*t}D_p/\nu$,
D_p = average particle diameter,
ρ_p = particle density,
g = gravitational acceleration, and
$\nu = \mu/\rho$ = fluid kinematic viscosity.

Equation (6a) holds for $0.22 \leq B \leq 10$. The variable A is the threshold coefficient. The variable B is the particle friction Reynolds number. For the range $B \leq 0.22$, Eq. (6b) applies:

$$A = 0.266\left(1 + 0.055/\rho_p gD_p^2\right)^{1/2} \times \left(1 + 2.123B\right)^{-1/2} . \tag{6b}$$

Equations (6a) and (6b) collapse the threshold friction speed data in the appropriate range of B onto a single curve with D_p and ρ_p as parameters. Given a particular aerosol size and density, we can calculate u_{*t} from Eq. (6a)

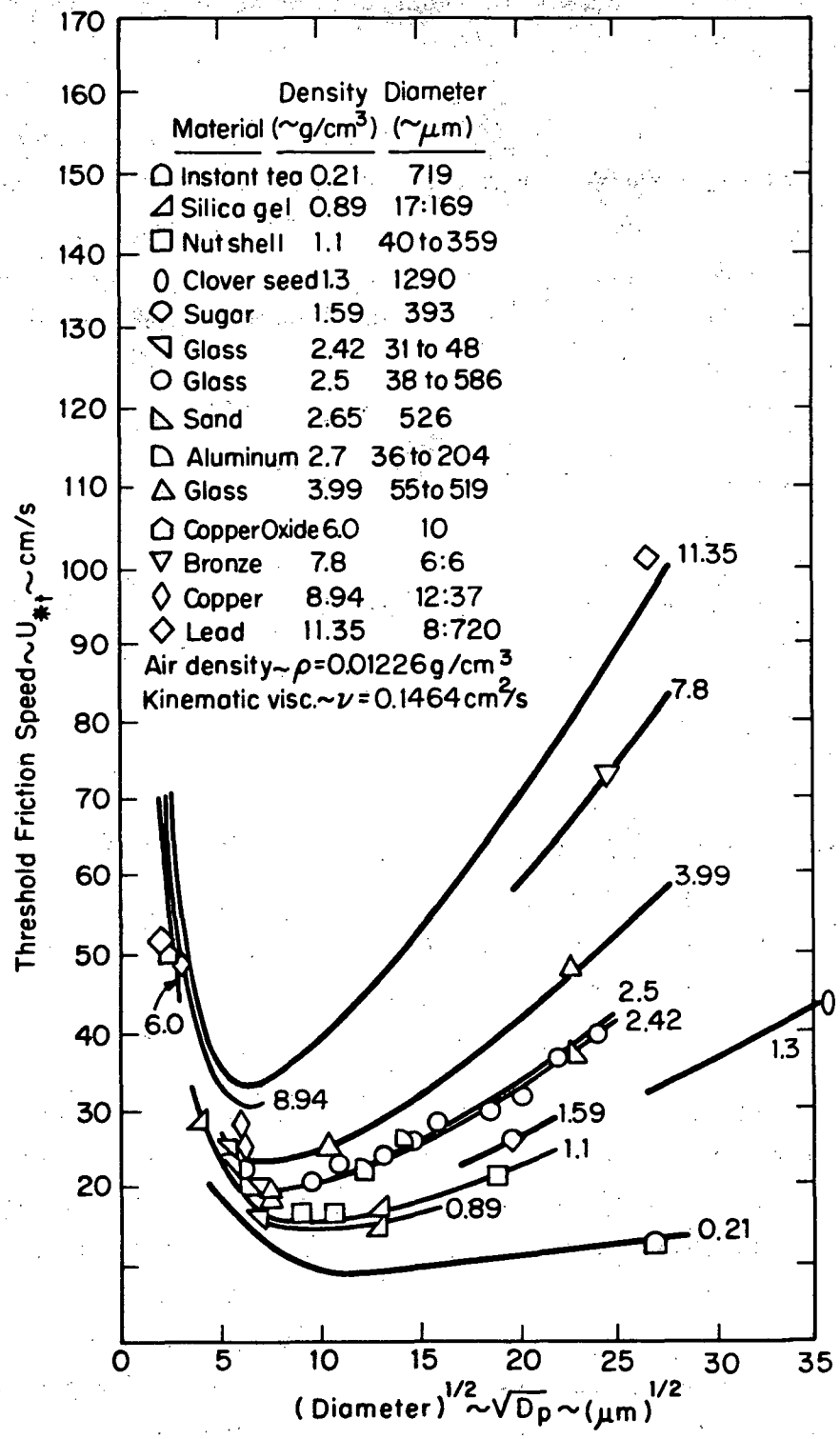

Fig. 2.
Particulate threshold friction speed.

and Eq. (6b). An iterative technique is used to solve for u_{*t} because this variable appears implicitly on both sides of the equations. The value of ν was assumed to be constant at $\nu = 0.1454$ cm^2/s, which corresponds to standard atmospheric conditions.

In u_{*t} we have a measure of when particle motion will occur and when entrainment is possible. Under given flow and surface conditions, a value of the friction velocity exceeding the threshold friction velocity can produce entrainment; that is, entrainment can occur only when $u_* > u_{*t}$. We may relate u_* to the corresponding velocity at the turbulent boundary layer edge using one of the following two equations. For a smooth surface with a laminar sublayer,[41]

$$u(y)/u_* = (1/0.41)\ \ln\ (yu_*/\nu) + 5.0 \quad . \tag{7}$$

For a rough surface with no laminar sublayer,[42]

$$u(y)/u_* = (1/k)\ \ln\ (y/y_0) \quad , \tag{8}$$

where y = distance from surface,
$k = 0.4$ = Von Karman constant,
$y_0 = R/30$ = roughness length, and
R = average surface roughness height,

and where the velocity $u(y)$ is calculated by the gas-dynamics module of the code. For a duct with fully developed turbulent airflow conditions, the centerline velocity or velocity at the boundary layer edge may be 25% higher than the average or bulk velocity. This version of the codes uses Eq. (8) for a rough surface with an assumed boundary layer thickness of $y = 10$ cm and a roughness length of $y_0 = 0.0104$ cm (a moderately rough surface). Our use of Eq. (8) will lead to higher values of u_* for the same values of $u(y)$ and y than Eq. (7). Because entrainment is known to depend on the difference $(u_* - u_{*t})$, our choice of Eq. (8) will lead to conservative estimates of entrained material.

The next question is "What determines whether particles go into suspension?" That is, of all the particles, how do we divide those that could become

airborne from those that remain close to the surface? Iversen et al.[40] have shown that for particles smaller than 52 μm, suspension occurs as soon as the threshold speed is reached. The criterion assumed here was that suspension will occur for those particles for which $u_s/u_* = 1$ and $u_* > u_{*t}$, where u_s is the particle fall or terminal speed. The friction speed u_* is of the same order of magnitude as the vertical component of turbulence in a boundary layer. Values of $D_p < 50$ μm for suspension are in agreement with measurements using soils.[38] In each code we have assumed that all of the particles are subject to suspension.

How much material becomes suspended? Travis[38] has suggested the following expression for q_v, the mass of particles per unit area per unit time that go into suspension.

$$q_v = q_h \left(c_v/u_{*t}^3 c_h\right) \left[(u_*/u_{*t})^{P/3} - 1\right] \quad , \tag{9}$$

where P = mass percentage of suspendable particles, and
c_v, c_h = empirical constants (2×10^{-10} and 10^{-6}, respectively).

In Eq. (9), q_h is the mass of material moving horizontally through a vertical plane perpendicular to the surface per unit width per unit time and may be determined from[43]

$$q_h = 2.61(\rho/g)(u_* + u_{*t})^2(u_* - u_{*t}) \quad . \tag{10}$$

The calculated aerodynamic entrainment option of the material transport module is a subroutine that uses Eqs. (6) through (10). The steps can be summarized as follows. At a given time, the gas-dynamics module supplies the velocity u(y) for every room or duct with material subject to aerodynamic entrainment. This value of u(y) and the turbulent boundary layer velocity profile in Eq. (8) are used to compute a surface friction velocity u_*. A characteristic value of threshold friction velocity u_{*t} for the input material characteristics is obtained from Eq. (6). If $u_* \leq u_{*t}$, no entrainment occurs. [See Eq. (10).] If

$u_* > u_{*t}$, then semi-empirical entrainment equations [Eqs. (9) and (10)] are used to estimate the vertical flux of suspendable material q_v. Knowing q_v and the floor area A over which the contaminant is uniformly distributed, we can compute the source term

$$\dot{M}_p = q_v A \quad , \tag{11}$$

which has the units kilograms per second. As a source term, Eq. (11) represents a positive contribution to the $\dot{M}_p$ term on the right-hand side of Eq. (29) in Sec. V. The floor area A is assumed to be flat and free of obstacles or protuberances.

The question of how heavily a surface must be loaded before equations like Eqs. (6), (9), and (10) are applicable is debatable. For realistic types of loadings, such as we expect to find in many locations of a fuel cycle facility, the empirical constant in Eq. (10) may not be satisfactory because it was obtained for relatively thick powder beds. Furthermore, the empirical coefficients in Eq. (9) are suspect because they were obtained from experiments with soil particles.

The recent experimental and theoretical work underlying Eqs. (6) and (10) is believed to be the best available.[39,40,43] Thus, the basis for predicting u_{*t} using Eq. (6) is sound; however, the data base to which Eq. (6) was fit is sparse for small, heavy particles. In principle, these uncertainties could be checked and reduced with appropriate experimentation.

C. Future Improvements

We believe that considerable analytical and experimental work is needed to support the area of material transport initiation. The current fuel cycle facility safety research program[1,2] is sponsoring investigative work in this area at both Los Alamos and PNL. At Los Alamos, one analytical task involves assessing existing compartment fire models for their ability to predict convective heat release rates (or fire compartment gas temperatures) and particulate and flammable gas mass release rates. In addition, Los Alamos is developing a new compartment fire model directed specifically at predicting the above parameters for the case of under-ventilated (oxygen-depleted) fires.[44] Established fire

models and laboratory oven test methods have not simulated such fires yet. Future improvements should consist of coupling a compartment fire model to the existing FIRAC network analysis capability and obtaining supporting experimental data from laboratory ovens and compartments.

Additional experimental data are being obtained by Los Alamos in the area of powder or dust entrainment under simulated accident conditions.[1] Such data are needed for simulants for radioactive materials under conditions of pulsed and shock flow for both light and heavy surface loadings. These data can be used to improve the empirical coefficients in entrainment equations such as those in Sec. III.A.

PNL has surveyed source-term information in the areas of fires and explosions.[1,2] It is sponsoring experiments at Factory Mutual Research Corporation to determine the pyrolysis/combustion characteristics of solid and liquid combustible materials of interest in fuel cycle facilities.[2] In addition, PNL is conducting experiments to determine source-term quantities of radioactive aerosol under conditions of powder and liquid free-fall spills[45] and pressurized releases.[2]

V. CONVECTIVE TRANSPORT

A. Background

We have developed a simple material convection model capable of predicting airborne material distribution in a flow network and its release to the environment. (Radioactive or toxic material release to the environment from an accident is a major concern in nuclear facilities.) The convective transport model is based on the assumptions that the particle size is small and that its mass fraction is small relative to the gas mass in the same volume. This allows us to assume that the material and the gas form a homogeneous mixture and that they are in dynamic equilibrium. In this case, the gas-dynamic aspect of the problem is not affected by the presence of the airborne material, and the particulate or material velocity is the same as the gas velocity at any location and time. Consequently, the only relation needed to describe the motion of the material is the continuity equation. This model and the underlying assumptions are presented in more detail below.

B. Assumptions

The usual mathematical formulation for the motion of a multiphase, multicomponent material system is based on the concept of continuum mechanics with some pertinent qualifications.[13] We can obtain a set of partial differential equations for some macroscopic parameters with a few phenomenological descriptions of the stress, heat flux, and diffusion plus other formulations for the physical and chemical interactions among phases and components and with the boundary. Some of the relationships are either incomplete or not known yet. Depending on the range of interest, an extensive simplification may be necessary. The following assumptions are made to reduce the complexity of the problem, but they still allow us to meet our simple objective, namely, the capability of handling material transport without disturbing the main gas flow to any significant degree.

We define the material as any pneumatically transportable substance in a ventilation system. The material can be solid, liquid, or even gas other than the main gas stream. The individual material point is assumed to be quite small in size if it is in the condensed phase; a material cloud is an ensemble of material. Throughout the ventilation system, the main body of the gas and the material cloud form a mixture. The description of the flow system is based on the continuum point of view. In Sec. V we will neglect all chemical reactions and physical processes such as deposition, entrainment, coalescence, material break-up, evaporation, and condensation, but most of these processes are considered in other sections of this report. Material generation is a prescribed quantity. Once the material cloud is formed and mixed with the main gas stream, our attention will be on the movement of the material.

Even in a dusty cloud, the volume occupied by the material is quite small compared with the volume of the gas. We will assume this is the case in our first model and refer to it as the disperse condition. A consequence of this is that the material motion is dominated by the aerodynamic forces (mainly drag) but not by the interparticle forces. Furthermore, the material size we most often encounter in a ventilation system falls into the micron range. For that small size, the aerodynamic relaxation time is quite small compared with the typical residence time. This means the material can respond quickly to the variation of gas velocity, and most of the time the material would have a velocity nearly identical to the gas at any location and time. Thus, we have obtained the dynamic equilibrium condition between the gas and the material cloud,

and the only equation that is needed to find out the material flow rate is the material continuity equation. We can add one more equilibrium condition (that is, the material temperature is the same as the gas), and we have a homogeneous equilibrium model for the gas and material cloud mixture. This mixture can be treated as a simple gas with the proper thermodynamic and transport properties used in all usual gas-dynamic equations.[46]

In principle, we could proceed to solve the set of gas-dynamic equations for the mixture. However, the mixture transport properties are not easy to determine. On the other hand, we still can obtain governing equations for the main gas stream and the material cloud separately. Some of these equations will contain terms that express the effect of interaction between the gas stream and the material. A closer examination of these terms reveals that if the material mass fraction is quite small compared with that of the gas, the effect of the interaction on the gas-phase flow is negligible. This is the disperse condition for the material cloud relative to the gas mass, and we will assume so. At this point, we have achieved the complete separation of the gas-phase flow dynamics from the material cloud. The gas-dynamic aspect of the material transport problem can be solved first, and then the continuity relation of the material will be used to determine the material flow. A more complete presentation of various multiphase, multicomponent flow problems is given in the literature.[13,46,47] All of the above assumptions and steps leading to the final simplification of the material transport problem are based on the literature cited.

C. Continuity Equation

In a volume V, a part of it is occupied by material with mass M_p and volume V_p and the rest by gas of mass M_g and volume V_g. Obviously,

$$V = V_p + V_g \quad . \tag{12}$$

We define a volume fraction of the material as

$$\alpha_p = \frac{V_p}{V} \tag{13}$$

and the densities (concentrations) of the material and gas based on the mixture volume as

$$\rho_p' = \frac{M_p}{V} \quad \text{and} \quad \rho_g' = \frac{M_g}{V} \ , \tag{14}$$

which differ from the densities based on the volume of the individual phase,

$$\rho_p = \frac{M_p}{V_p} \quad \text{and} \quad \rho_g = \frac{M_g}{V_g} \ . \tag{15}$$

Only ρ_g is related to the pressure and temperature through the equation of state. The mass fraction of the material is defined as

$$Y_p = \frac{M_p}{M_p + M_g} \ . \tag{16}$$

We can express the mass fraction in terms of volume fraction through the following relation.

$$Y_p = \left[1 + \left(\frac{1-\alpha_p}{\alpha_p}\right) \left(\frac{\rho_g}{\rho_p}\right)\right]^{-1} \ . \tag{17}$$

Because the material-phase density of liquids or solids is usually so much larger than the gas-phase density, the disperse condition ($\alpha_p << 1$) does not imply the dilute condition ($Y_p << 1$) unless

$$\alpha_p << \frac{\rho_g}{\rho_p} \ , \tag{18}$$

which is a more stringent condition. We will assume this is the case in the current material convection model.

The velocity of a mixture is defined as follows.

$$\underline{u} = (\rho_p' \underline{u}_p + \rho_g' \underline{u}_g) / \rho \quad , \tag{19}$$

with

$$\rho = \rho_p' + \rho_g' \quad . \tag{20}$$

ρ is the density of the mixture. $\underline{u}$, $\underline{u}_p$, and $\underline{u}_g$ represent the mixture velocity, material velocity, and gas velocity, respectively; they are vector quantities. Using the mass fraction Y_p, we have

$$\underline{u} = Y_p \underline{u}_p + (1-Y_p)\underline{u}_g \quad . \tag{21}$$

If u_ρ and u_g are of the same order of magnitude and for the dilute condition,

$$\underline{u} \cong \underline{u}_g \quad . \tag{22}$$

The mixture velocity is dominated by the gas velocity. Also from Eq. (20), the mixture density is roughly the same as the gas density. We expect this should be the case for a light loading situation. From now on, we will drop the subscript g for all quantities associated with the gas phase.

The continuity equation for any phase or component in a mixture is[47]

$$\frac{d}{dt}\int_V \rho_p' dV = - \int_S \rho_p' \underline{u}_p \cdot d\underline{S} + \dot{M}_p \quad . \tag{23}$$

The time derivative term on the left-hand side represents the change of the material density inside a control volume V. The first term on the right-hand side is the material flow through the boundary S of the volume V, and the last term is the material source. Assuming ρ'_p is uniform over the control volume and using the same representation we have for the gas continuity equation, Eq. (23) becomes

$$V \frac{d\rho'_p}{dt} = \sum_i \rho'_{pi} u_{pi} A_i + \dot{M}_p \quad . \tag{24}$$

Here we drop the vector notation for the velocity but add the subscript i to indicate the flow path connecting to that volume. A_i is the flow area, and u_{pi} is the flow velocity normal to the area. The positiveness of the flux term is referred to as the flow into the volume. Again we introduce Y_p into Eq. (24),

$$V \frac{d}{dt} [Y_p \rho] = \sum_i Y_{pi} \rho_i u_{pi} A_i + \dot{M}_p \quad , \tag{25}$$

or

$$V \frac{dY_p}{dt} = \frac{1}{\rho} \left[\sum_i Y_{pi} \rho_i U_{pi} A_i + \dot{M}_p - Y_p V \frac{d\rho}{dt} \right] \quad . \tag{26}$$

The last term in Eq. (26) is the gas density change and is determined by the gas continuity equation.

Under the dynamic equilibrium condition, the material velocity is almost identical to the gas velocity everywhere and at any instance, namely,

$$u_{pi} = u_i \quad . \tag{27}$$

u_i represents the gas velocity in pathway i. Substituting that into Eq. (26) and recalling the gas mass flow in branch i,

$$\dot{m}_i = \rho_i \, u_i \, A_i \quad , \tag{28}$$

we obtain

$$V \frac{dY_p}{dt} = \frac{1}{\rho} \left[\sum_i Y_p \, \dot{m}_i + \dot{M}_p - Y_p \, V \, \frac{d\rho}{dt} \right] . \tag{29}$$

Equation (29) is a differential equation for the unknown Y_p. Once the gas-dynamic quantities ρ and $\dot{m}_i$ are known, Eq. (29) can be integrated to obtain Y_p at a new time. The advantage of using Y_p instead of ρ_p as the unknown is that Y_p is not subject to the effect of compressibility as is ρ_p. Once Y_p is calculated, the material density concentration can be obtained through

$$\rho_p' = Y_p \, \rho \quad . \tag{30}$$

The quantity mass fraction (or molar fraction) has been used extensively in fluid flow with chemical reaction. In the TORAC code, we expect the air density variation to be small, so we use Eq. (24) in the numerical calculation directly without referring to the mass fraction step.

Finally, we must emphasize again that the assumptions that are made about the dilute condition of the material enable us to solve the gas-dynamic problem independently. The validity of the assumptions depends on the individual case that we are facing. However, we do believe that this simple model will cover a broad range of problems related to material movement in nuclear facilities.

VI. AEROSOL INTERACTION

A. Background

One goal of the fuel cycle facility safety analysis program is to predict the quantity and physical and chemical characteristics of radioactive material that could be transported to a plant boundary. Unfortunately, the quantity and physical and chemical characteristics of the material can be changing, especially during the course of an accident. In particular, the aerosol mass in the respirable size range at the time of exhaust at a facility boundary can be quite different from that produced near the accident. An intermediate need is to predict the quantity and characteristics of aerosols that reach the nuclear filtration systems (or other engineered safeguards) because this can affect the filter plugging behavior. Further, aerosol characteristics are needed to model transport processes because size and density play a role in determining what type of deposition mechanisms will be important as well as in determining the magnitude of the deposition flux or aerosol depletion (Sec. VII). Thus, aerosol interaction dynamics are an essential aspect of material transport.[9] This is especially true for conditions of high aerosol concentration (10^6 particles/cm^3 or greater). In nuclear fuel cycle facilities, high aerosol concentrations could result from the accidents under study (particularly fires). For explosions, high concentrations are more likely to occur in the near-field, that is, close to the actual explosion.

The general dynamic equation (GDE) is a nonlinear, partial integro-differential equation that models the time rate of change of the size distribution of an aerosol.[9,48] The GDE can be formulated for continuous or discrete size distribution functions.[49] The continuous GDE may be written for a spatially and chemically homogeneous system consisting of a single aerosol species in the absence of convection.[9,48]

$$\frac{\partial n(v,t)}{\partial t} = -\frac{\partial}{\partial v} I(v,t)n(v,t) + \int_0^{v/2} \beta(v-u,u)n(v-u,t)n(u,t)du - n(v,t)\int_0^{\infty} \beta(v,u)n(u,t)du + S\left[n(v,t),v,t\right] \quad , \tag{31}$$

where $n(v,t)$ is the size distribution density function so that $n(v,t)dv$ is the number of particles per unit volume of fluid with volumes in the range v to $v + dv$. In Eq. (31), $I(v,t) = dv/dt$, the rate of change of the volume of a particle of volume v by transfer of material between the particle and the fluid phase, $\beta(v,u)$ is the coagulation coefficient for particles of volumes v and u, and S is the net rate of addition (or removal if $S < 0$) of particles into the system. Equation (31) states that during a process, mass is conserved throughout the aerosol population size distribution.

The first term on the right-hand side of Eq. (31) represents the rate of growth or shrinkage of particles by gas-to-particle conversion (including gas-phase chemical reactions and condensation). The second term represents the coagulation gain of particles in the size range $(v,v + dv)$ by collision of two particles of volumes $v - u$ and u to form a particle of volume v. The third term represents the coagulation loss of particles in the size range $v + dv$ by collision with all other particles. Finally, the last term represents all particle sources and sinks.

B. Future Plans

The current versions of TORAC, EXPAC, and FIRAC do not allow material interaction, but future versions should provide this capability using existing physical models for the terms in Eq. (31). However, although solutions to Eq. (31) are difficult to obtain, analytical solutions to a few simple forms of the initial condition [$I(v,t)$, $\beta(v,u)$, and S] are available. Some analytical solutions are reported in Refs. 9 and 48, including cases of coagulation alone and simultaneous coagulation plus removal, coagulation plus growth, and turbulent diffusion and growth. Although the analytical solutions to Eq. (31) may not correspond directly to realistic physical conditions, they may be useful as first approximations and also serve to check the accuracy of numerical solutions.[50,51]

There is a major step from single-species models to multispecies models. References 52 and 53 present the analytical and numerical developments currently being used in the multicomponent aerosol computational technique MAEROS, which was developed by F. Gelbard. These techniques are being assessed for possible use in this program. Research in the area of aerosol dynamics currently is very active.

VII. AEROSOL DEPLETION

A. Background

Because the flow Reynolds number based on the enclosure or duct hydraulic diameter and fluid bulk velocity will be greater than about 2100 for all cases of interest here, the flow always will be turbulent. We will assume that all flows are developed fully so that boundary layer or duct velocity profile shapes are constant with distance. This will be true sufficiently far from inlets (20 to 50 hydraulic diameters) so that entrance effects are unimportant in our calculations.

Under these conditions, not all of the material that is made airborne at the location of material transport initiation will survive convective transport to the filtration systems or facility boundary. Depending on the aerosol aerodynamic characteristics and passage geometry, there may be a sizable reduction in aerosol concentration. As such, an enclosure or duct acts as an aerosol filter.

B. Existing Capability

Once the user has chosen to exercise material transport, he can calculate aerosol losses caused by gravitational sedimentation in rooms, cells, and horizontal rectangular ducts in this version of our codes. This module can be turned on for rooms and horizontal ducts and turned off for vertical ducts by adjusting input flags. Aerosol depletion may be calculated throughout the network during transient flow. The theory is based on quasi-steady-state settling with the terminal settling velocity corrected by the Cunningham slip factor. The flow in ducts and rooms is assumed to be well-mixed so that the aerosol concentration is uniform within the volume. More detail and references may be found below. The user must supply only the aerosol diameter and density to this model, and the aerosol may consist of solid particles or liquid droplets.

Future versions of the material transport module will account for combined molecular and turbulent diffusion as well as aerosol interactions, but the current version is restricted to gravitational sedimentation. The particle flux J resulting from gravitational sedimentation is[9]

$$J = u_s n \quad , \tag{32}$$

where the units of J are particles per unit area per unit time, u_s is the terminal settling velocity or transfer coefficient for sedimentation, and n is the local aerosol number concentration in particles per unit volume for the homogeneous aerosol. If we multiply both sides of Eq. (32) by the homogeneous particulate mass m_p, then

$$J' = u_s \rho_p' \quad , \tag{33}$$

where the units of J' are mass per unit area per unit time and $\rho_p' = nm_p$ is the aerosol mass concentration per unit volume. The terminal settling velocity is calculated from[9]

$$u_s = \rho_p D_p^2 gC/18\mu \quad , \tag{34}$$

where ρ_p = aerosol density,
D_p = aerosol diameter,
g = gravitational acceleration,
C = Cunningham slip correction factor, and
μ = fluid dynamic viscosity.

The code input variables for material depletion are ρ_p and D_p. These variables may be assumed by the user. We recommend that the user select aerodynamic diameter with unit density or Stokes diameter with the material bulk density. This selection was discussed in Sec. VII.A above. To calculate the slip correction factor, the code uses[9]

$$C = 1 + \left(2L/D_p\right)\left(A_1 + A_2 \exp(-A_3 D_p/L)\right) \quad , \tag{35}$$

where L is the molecular mean free path and the A's are dimensionless constants based on experimental measurements of small particle drag. The code uses

$$
\begin{aligned}
L &= 0.065\ \mu m, \\
A_1 &= 1.257, \\
A_2 &= 0.400, \\
A_3 &= 0.550, \\
g &= 981\ cm/s^2, \text{ and} \\
\mu &= 0.0001781\ g/cm\text{-}s,
\end{aligned}
$$

where L, μ, and g are taken at standard sea-level conditions.

We know ρ_p' from the material transport mass balance calculation for the previous time step for each node (volume or duct). Then, knowing u_s and the projected floor area for sedimentation A, we can compute the sink term using Eq. (33),

$$\dot{M}_p = -J'A = -u_s \rho_p A' , \tag{36}$$

which has the units kilograms per second. Because aerosol depletion is a sink term, we have used a minus sign in Eq. (36). This equation represents a negative contribution to the $\dot{M}_p$ term on the right-hand side of Eq. (29). Aerosol depletion by sedimentation may be selected for all volumes and ducts and is calculated in the same manner.

C. Future Improvements

Aerosols moving through passages that are horizontal (or not exactly vertical) can be deposited because of gravitational settling. However, a number of other processes that can cause aerosol depletion and contribute to a material transport sink term should be considered.[9-11,14] Particles that come sufficiently close to surfaces can be intercepted mechanically and stuck. Particles with enough inertia can deviate from the flow streamlines, impact, and stick to rough elements, obstacles, or bends. Particles less than about 1 μm in size can be transported to surfaces by both turbulent (eddy) and molecular (Brownian)

diffusion. Particles greater than about 1 μm in size and being transported parallel to surfaces can be deposited because of the fluctuating velocity components normal to the surface (turbulent inertial deposition). Lower flow velocities enhance deposition caused by molecular diffusion and sedimentation. Unless the surfaces are sticky, the net rate of deposition will depend on the relative rates of transport and reentrainment. Except for fibrous particles or very light particles, interception may be neglected because particles large enough to be intercepted will most likely be deposited as a result of inertial effects or sedimentation.

Under certain conditions, other effects may become important for the smallest particles. These effects include thermophoresis, diffusiophoresis, and electrical migration. The latter three effects are discussed in Refs. 9 and 14. They are believed to be relatively unimportant here compared with other effects.

Friedlander's book[9] provides an excellent introduction to deposition by convective diffusion and inertial deposition. Here the concept of a particle transfer coefficient k is introduced such that

$$J = k\, n_0 \quad , \tag{37}$$

where J is the particle deposition flux (particles per square centimeter-second) at a given location in a tube and n_0 is the local average particle number concentration (particles per cubic centimeter) in the mainstream at that cross section. Thus, the transfer coefficient k has units of centimeters per second and may be considered an effective deposition velocity. Experimental measurements of k for liquid droplets and solid particles were obtained for turbulent flow in vertical tubes at Reynolds numbers up to 50 000.[54,55] Several theories for predicting k for turbulent deposition are based on the "diffusion free-flight" model. Particles are assumed to be transported by turbulent diffusion to within one "stopping distance" from the wall, at which point the particles make a "free flight" to the wall. The stopping distance is

$$s = \bar{v}\tau = \rho_p D_p^2 \bar{v}/18\mu \quad , \tag{38}$$

where τ is the particle relaxation time and $\bar{v}$ is the assumed free-flight velocity.

Beal[56] has developed a method of analysis for predicting k for turbulent flow in vertical tubes. Beal's method combines the approaches taken in Refs. 54 and 57 and applies them to particles ranging from molecule size to about 100 μm. This theory accounts for the deposition mechanisms of Brownian and turbulent diffusion and turbulent inertial deposition but not gravitational settling. Beal's approach is to integrate the particle flux equation

$$J = (D + \epsilon)\frac{dn}{dy} \tag{39}$$

across the concentration boundary layer. Here D is the particle coefficient of molecular diffusion, and ϵ is the particle eddy diffusivity (both with units of square centimeters per second). In the derivative, y represents distance in centimeters perpendicular to the surface. In the paper Beal[56] states his assumptions for $\bar{v}$ and ϵ in specific regions of the turbulent boundary layer and derives equations for k.

The authors of Ref. 58 have developed a method for predicting k for turbulent flow in horizontal tubes. This method applies to particles with a size greater than about 1 μm because it accounts for the deposition mechanisms of turbulent diffusion and gravitational settling but does not account for Brownian diffusion. Reference 58 also considers the effect of pipe wall roughness and provides experimental verification for particles with sizes from about 1 to 4 μm.

The equations for k presented in Refs. 56 and 58 were incorporated into a computer code called DUCT[8] that estimates aerosol depletion under steady flow conditions in a given duct segment. We propose to include these equations as an improvement to the aerosol depletion modules in TORAC, EXPAC, and FIRAC.

Experimental data are needed to check aerosol depletion calculations for losses encountered in larger scale facilities, particularly for fire conditions. Such data are being sought in the current fuel cycle safety program. Another area needing improvement is accounting for the effects of other ventilation system components (besides filters) such as blowers, dampers, bends, and flow restrictions on aerosol removal.

VIII. FILTRATION

A. Background

A phenomenological approach to filter loading is used. The filter gas-dynamic performance can be changed by the accumulation of airborne material on the filter, which in turn causes an increase in resistance. A linear model is used in which the increase in resistance is linearly proportional to the amount of material on the filter. The proportionality constant is a function of both material and filter properties. The user supplies the filter efficiency and plugging factor; however, the information for the latter is not readily available in the literature.

Experimental evidence[59] indicates that the pressure drop across filters commonly used for air cleaning in the chemical and nuclear industries increases nonlinearly at high-speed flow. This contrasts with the linear relationship that we generally observe in a relatively low-speed flow region for normal or near-normal applications.[6] We can take an entirely experimental approach to determine all of the influence coefficients on filter and flow properties, or we can model the filter flow based on the principle of flow through porous media and determine the relationship between the flow rate and the pressure drop with most (if not all) pertinent parameters explicitly included. Even so, some empirical constants still are needed; for practical purposes, we can combine some filter properties into these constants and determine them by experimental means. The number of coefficients with proper filter modeling is much less than that obtained through direct empirical methods. We will review some theoretical works and present a model that is suitable for our system.

The purpose of air filters in a ventilation system is to remove airborne material in the air stream and to prevent hazardous material from being released to the environment. Experience shows that the accumulation of material, usually in the condensed phase, will cause the pressure drop across a filter to increase for the same flow rate. In the case of a fire or an explosion, rapid flow resistance increases as the result of large amounts of material caught by a filter. This is commonly called filter plugging or clogging. After reviewing analytical work on the development of filter models, we will review filter plugging phenomena briefly and eventually propose a semi-empirical formulation to describe this condition.

B. Filter Model

The pioneering work of D'Arcy[60] established the foundation of the principle of fluid flow through porous media. His experimental results indicated a linear relationship between the flow rate and the pressure drop that is proportional to an empirical constant, permeability. This parallels quite well Hagen-Poiseille's conclusion of fully developed laminar flow through a pipe.[42] It is not surprising to find that many theoretical models of flow through porous media are based on D'Arcy's concept but with different qualifications. The most successful one among them is the Kozeny model.[61] According to his theory, the porous medium is represented by an assemblage of channels of various cross-sections and a definite length. The flow through the channels is determined by the Navier-Stokes equations, and the permeability is expressed in terms of viscosity and the properties of the porous medium. However, an empirical constant is needed to include the effect of the tortuous characteristic of the medium. A modification of the Kozeny model by Carman[62] defined the constant, which is called tortuosity, in a more explicit way. This new model still requires an empirical coefficient to account for the uncertainty of determining various porous medium properties.

Another point of view on the pressure-drop relationship of flow through a porous medium is based on drag theory with the dragging obstacles being particles or fibers. A model using fibers as a porous medium leads to a permeability that is weakly dependent on flow rate.[63] Because of the actual complexity of the medium, some empirical adjustment is needed for this model.

So far we have discussed D'Arcy's law and its derivatives, which are adequate only when the flow velocity is low; that is, at conditions where the pressure drop is proportional to the viscous dissipation by the porous medium. For channel flow with flow velocity increasing, the dissipation mechanism changes from a viscous to a turbulent effect, and the pressure drop then is proportional to the kinetic energy of the stream.[42] Following the reasoning of Kozeny in modeling porous media as channels, we can establish a quadratic relation between the pressure drop and flow rate at high velocity.[64] Again, an empirical coefficient equivalent to the resistance factor in pipe flow under turbulent conditions is introduced. The summation of viscous effects and turbulent dissipation leads to an equation proposed by Ergun.[65]

$$\frac{\Delta p}{\ell} = 150 \frac{(1-\varepsilon)^2}{\varepsilon^3} \frac{\mu u_m}{d_p^2} + 1.75 \frac{(1-\varepsilon)}{\varepsilon^3} \frac{\rho u_m^2}{d_p} \quad , \tag{40}$$

with

Δp = pressure drop,
ℓ = bed length,
g = gravitational constant,
ε = void fraction,
μ = viscosity,
d_p = effective porous medium particle size,
ρ = fluid density, and
u_m = superficial velocity.

Superficial velocity is the flow velocity approaching the packed bed and not the average flow velocity in the interstitial region. Equation (40) is written in centimeter-gram-second units but also can be expressed in a different form,

$$\Delta p = K_L \mu \frac{Q}{A^{3/2}} + K_T \frac{\rho Q^2}{2A^2} \quad , \tag{41}$$

where Q and A represent volume flow rate and the frontal area of the packed column. It can be easily identified that

$$u_m = \frac{Q}{A} \quad , \tag{42}$$

$$K_L = 150 \frac{(1-\varepsilon)^2}{\varepsilon^3} \frac{\ell A^{1/2}}{d_p^2} \quad , \tag{43}$$

and

$$K_T = 3.5 \frac{(1-\epsilon)}{\epsilon^3} \frac{\ell}{d_p} \quad . \tag{44}$$

K_L and K_T are dimensionless and are dependent on the properties of the porous medium. Equation (41) is identical to the Reynolds' expression on pipe flow in laminar and turbulent regions.[66]

As we mentioned earlier, the theoretical model that we ultimately choose will use some empirical coefficients and must be included to account for the complexity and uncertainty of the porous medium. It does not matter if we obtain K_L and K_T first from Eqs. (43) and (44) and then add experimental corrections later. We can determine the effective K_L and K_T directly from experiment. This task is not more difficult than finding the correction factors alone because there are only two unknowns involved as presented in Eq. (41). From now on we will use Eq. (41) as the foundation of our filter model regardless of the filtration medium we use as long as we can determine the two coefficients through experimental or analytical means.

A subroutine using Eq. (41) to represent a filter branch has been added to the TORAC code because we expect very high flow rates in the system if a tornado-induced depressurization occurs. The turbulence coefficient K_T must be read in through the input file; if it is zero, then only the laminar-dependent portion will be used. The laminar coefficient K_L can be input or calculated for a given pressure drop and flow rate; the former approach is preferred. This subroutine has been checked out successfully. However, reliable data on K_T have not been obtained, and more extensive experimental work is needed in that area.

C. Filter Plugging

The physical phenomena involving the capture of an aerosol under flow conditions by a filtration medium are complicated.[67,68] The porous material provides various locations for material retention--bed grain surfaces, crevices, constrictions, or pore cavities. The normal pressure of the fluid, friction, interparticle forces, and the chemical bonding force give the required means of holding the material at a given location. The mechanisms for the suspended material reaching a retention site include gravity, inertia, hydrodynamic forces,

interception, and Brownian motion. Attempts to relate the overall filter efficiency with the aforementioned mechanisms without any experimental coefficient is not practical. A more useful approach is phenomenological; that is, we assume some form of dependence of filter efficiency on the total amount of aerosol retained. We note that experimentation indicates a small increase in the efficiency for increasing retention. For normal operating conditions, we assume that filter efficiency remains constant and does not significantly affect the system flow conditions.

The same conclusion cannot be drawn about the flow resistance of the filter when a large amount of material is retained on it. The increase in resistance can be quite substantial and should be dealt with properly. The plugging is related to material size, shape, phase, filter structure, and the quantity of captured material. Using the Carman-Kozeny filter model,[62] we can see that the material retention reduces the specific surface, which is defined as the total surface of the bed grain per unit filter volume and thus increases the effective resistance.[53] We can express the general relation as follows.

$$\frac{\Delta p}{(\Delta p)_o} = f(M_a) \quad , \tag{45}$$

where $(\Delta p)_o$ is the pressure drop for a clean filter, shown in Eq. (41), and f is a monotonically increasing function of material mass M_a on the filter. Clearly, $f(M_a = 0) = 1$. For a light loading condition, f is a linear function of M_a:

$$f(M_a) = 1 + \alpha M_a \quad , \tag{46}$$

where α is a coefficient dependent on filter and material properties.[68] More recent work of Bergman[69] using the fibrous drag model of Davies[70] concludes that α depends on the fiber volume fraction, fiber size, and particulate size. However, the foundation of Davies' model is still empirical. For the time being, we will postulate the phenomenological relation of Eq. (46) with α being determined by experiment. As future data warrant, we will modify the equation and include more explicit relations.

D. Future Improvements

We have presented the nonlinear filter and filter plugging models used in the TORAC computer code. The background physics, simplification, and mathematical formulation have been discussed and evaluated. We would not stop our effort here, and therefore, we are continuing to modify the codes and are adding various features to them as needed. We will complement our analytical effort with extensive experimental investigations to determine the effects of material type, moisture, and heat on α in Eq. (46) and on the form of the function f in Eq. (45).

IX. SAMPLE PROBLEMS USING TORAC

TORAC is an acronym for the Tornado Analysis Code. The code can predict tornado-induced flows, pressures, and material transport within structures. This computer code is primarily the TVENT computer code,[6] but it has been modified to include material transport, particularly the transport of radioactive material. This code is the first of a number of versions that will evolve into more refined and improved codes, and it is one code in a family of computer codes that is designed to provide improved methods of safety analysis for the nuclear fuel cycle industry.

TORAC solves steady-state and transient pressures and gas and material flow distributions in complex airflow pathways within structures. System pressures, flows, and material transport in this version of the code are based on the following assumptions.

- Isothermal flow
- Lumped-parameter formulation
- Incompressible flow with compressibility at nodes
- Gas dynamics decoupled from material transport
- No material interaction, phase change, or chemical reaction allowed during transport
- Homogeneous mixture and dynamic equilibrium
- Material deposition only by the mechanism of gravitational settling
- Material entrainment based on resuspension factor and other concepts for rooms and semi-empirical entrainment rate equations and wind tunnel data for ducts

A single file containing the input for all the sample problems appears as a subroutine at the end of the TORAC[3] source program. The user may execute this

file "as is" to run the "Tornado at Exhaust" condition. Nine other sample problems can be run from this same file by following the instructions given in comment statements at the end of the file. The hypothetical ventilation system used in these problems is shown in Fig. 3. It consists of a supply and exhaust blower, a large room, dampers, a filter plenum, a long duct, and an exhaust stack. The corresponding computer model is shown schematically in Fig. 4. The purpose of these sample problems is to demonstrate the capabilities of the various program features. The sample problems do not necessarily reflect realistic situations.

This input file (Fig. 5), which is at the end of TORAC, is written to a file called INPUT if the TORAC program is executed without the existence of a file called INPUT. The test for this file is made automatically if the file-search utility is available. If this is not the case, the user must change the source program for the initial run only to write the input file rather than reading from one in your local file space.

The sample problems appearing in this combined input file are (1) Tornado at Exhaust, (2) Tornado at Intake, (3) Supply Blower Turned Off and On, (4) Supply Blower Speed Reduced, (5) Control Damper Closing and Blower Speed Reduced, (6) Material Transport (No Filter Plugging), (7) Material Transport (Filter Plugging), (8) Entrainment, and (9) Deposition. Here we will provide examples pertaining to material transport only.

The sample problems presented here demonstrate the following program features using the system shown in Figs. 3 and 4.

- Material transport
- Filter plugging
- Entrainment
- Deposition

A tornado is simulated by specifying a pressure-time function at one or both boundary nodes. This will be illustrated in the sample problems below. Up to 20 points can be used to define the assumed fluctuations in pressure that simulate the passing of a tornado. A blower is turned off by replacing the blower with a damper having a known resistance characteristic. Blower characteristics are changed during a run by substituting another blower curve at the time the change occurs. A damper is closed or opened according to a given resistance coefficient time function for that branch. These features can be made to occur at different intervals during a run to depict a sequence of events. Material

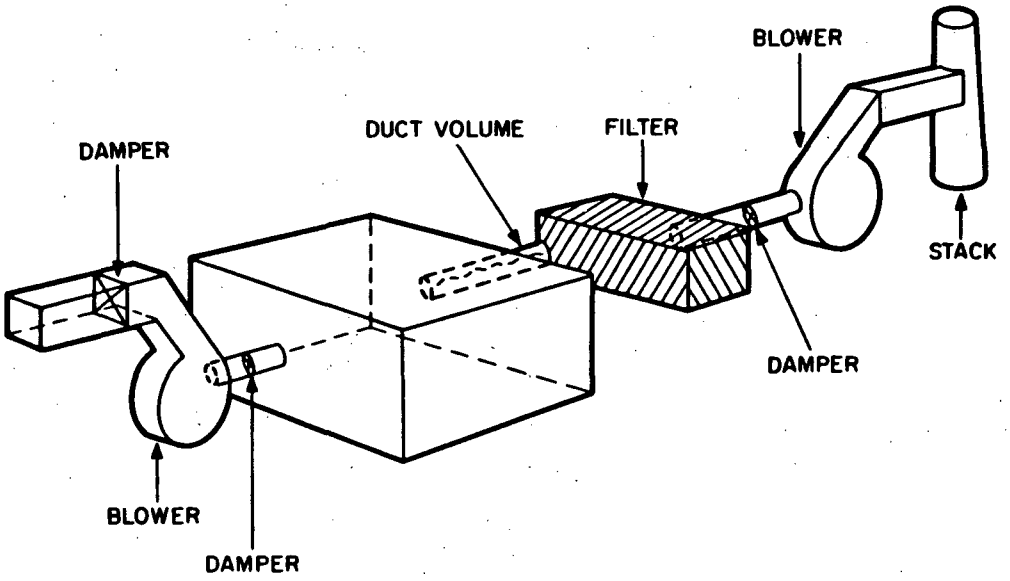

Fig. 3.
TORAC sample problem ventilation system schematic.

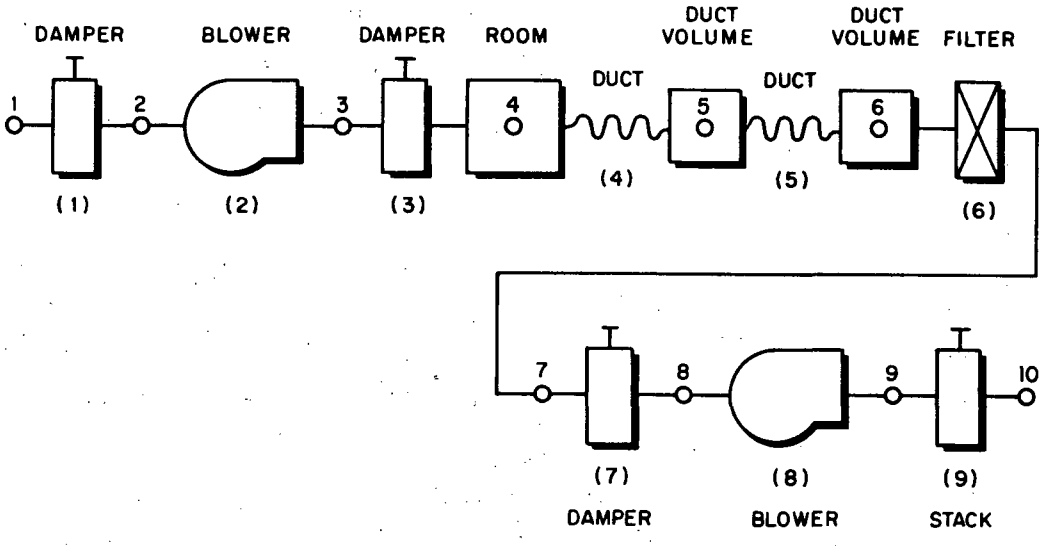

Fig. 4.
Computer model of TORAC sample problem ventilation system.

```
*
EXAMPLE PROBLEMS (E.G. TORNADO AT EXHAUST)
*
* RUN CONTROL 1
   ST  0.0  .01 030.                                                    0    0    0
* PRINT/PLOT CONTROL                          PLOT OPTION NO. 2
        3    1    1                            "    "    "  2
* FRAME DESCRIPTIONS                          "    "    "  2
    4    2    3    4    5                     "    "    "  2
    4    6    7    8    9                     "    "    "  2
    2   10    1                               "    "    "  2
    4    2    4    6    8                     "    "    "  2
    3    2    6    8                          "    "    "  2
* RUN CONTROL 2
  500                          P   1    1
* BOUNDARY CONTROL
    1    2                         1    1    1
* GEOMETRY AND COMPONENT CONTROL
    9   10         3    3    1
* BRANCH DATA
    1    1    2 1000.                          V
    2    2    3 1000.                          B                        1
    3    3    4 1000.                          V
    4    4    5 1000.                          V
    5    5    6 1000.                          V
    6    6    7 1000.                          F                             0
    7    7    8 1000.                          V
    8    8    9 1000.                          B                       2
    9    9   10 1000.                          V
* BOUNDARY DATA
    1              0
   10              1
* CONTROL DAMPER INSTRUCTIONS
    1
    0    1   4.000E-07  9
* BLOWER CURVE CHANGE INSTRUCTIONS
    1
    0    3  50.   2
* TORNADO PRESSURE FUNCTION
    1    5
0.0         0.0        10.        0.0        12.        -25.
16.         -25.       18.        0.0
* PARTICULATE FUNCTION
    1    6 0.35
0.0         0.0        10.        0.0        12.        0.1
14.         0.1        15.        0.0        60.        00
* CONTROL DAMPER FUNCTION
    1    4
0.0             4.000E-07  80.          4.000E-07  100.          1.000E-06
150.            1.000E-06
* BLOWER TURNED OFF/ON INSTRUCTIONS
    1
    0  50.      1.000E-09 150.        2
* ROOM DATA
    4 10.       10.        10.         0
    5  2.        2.        50.
    6  2.        2.        50.
* FILTER MODEL DATA
    1    1
   .8
  0.0
* BLOWER CURVES
    1    6
-100.      2.7       0.0       1.9       800.      1.8
```

Fig. 5.
Built-in TORAC input file.

```
 65 1000.       1.6        1300.      0.8        1400.      0.0
 66     2    6
 67 -200.       1.4        0.0        1.0        700.       0.9
 68 1000.       0.7        1400.      0.4        1600.      0.0
 69     3    6
 70 -100.       2.3        0.0        1.6        770.       1.5
 71  940.       1.3        1100.      0.8        1200.      0.0
 72 * PRESSURES
 73      0.0              -0.5             +1.1             1.0              0.9
 74      0.8              -0.2             -0.3             0.4              0.0
 75 * DEPOSITION COEFICIENTS
 76
 77     0    0    0    0   0.0       0.0
 78     0    0    0    1   0.0       0.02
 79     0    0    0    1   0.0       0.02
 80 END OF INPUT FILE.  ANYTHING WRITTEN BEYOND THIS POINT WILL BE IGNORED
 81 WHEN THIS FILE IS READ.
 82
 83 REPLACE LINES 6 THRU 13 WITH ONE OF THE FOLLOWING OPTIONS
 84
 85 * PRINT/PLOT CONTROL                          PLOT OPTION NO.  1
 86          2    1    1                            "      "     "   1
 87 * FRAME DESCRIPTIONS                            "      "     "   1
 88     4    2    3    4    5                       "      "     "   1
 89     4    6    7    8    9                       "      "     "   1
 90     4    2    4    6    8                       "      "     "   1
 91     3    2    6    8                            "      "     "   1
 92
 93 * PRINT/PLOT CONTROL                          PLOT OPTION NO.  2
 94          3    1    1                            "      "     "   2
 95 * FRAME DESCRIPTIONS                            "      "     "   2
 96     4    2    3    4    5                       "      "     "   2
 97     4    6    7    8    9                       "      "     "   2
 98     2   10    1                                 "      "     "   2
 99     4    2    4    6    8                       "      "     "   2
100     3    2    6    8                            "      "     "   2
101
102 * PRINT/PLOT CONTROL                          PLOT OPTION NO.  3
103                    1    1    1    1             "      "     "   3
104 * FRAME DESCRIPTIONS                            "      "     "   3
105     1    6                                      "      "     "   3
106     3    3    4    5                            "      "     "   3
107     4    4    5    6    7                       "      "     "   3
108     4    4    5    6    7                       "      "     "   3
109
110 THE FOLLOWING RUNS CAN BE MADE FROM THE ABOVE INPUT FILE BY MAKING THE
111 CHANGES INDICATED
112
113 RUN          CHANGES TO "COMBINED INPUT FILE"
114 ---          --------------------------------
115
116  TORNADO AT EXHAUST (PLOT OPTION NO. 2)
117       "AS IS"
118
119  TORNADO AT INTAKE (PLOT OPTION NO. 2)
120       LINE 32 - 1 TO 0 (CC 20)
121       LINE 31 - 0 TO 1 (CC 20)
122
123  SUPPLY BLOWER TURNED OFF AND ON (PLOT OPTION NO. 1)
124       LINE 5 - 030. TO 200.
125       LINE 32 - 1 TO 0 (CC 20)
126       LINE 53 - 0 TO 2 (CC 5)
127
128  SUPPLY BLOWER SPEED REDUCED (PLOT OPTION NO. 1)
```

Fig. 5.
Built-in TORAC input file (cont).

```
129       LINE 5 - 030. TO 200.
130       LINE 32 = 1 TO 0 (CC 20)
131       LINE 38 - 0 TO 2 (CC 5)
132
133  CONTROL DAMPER CLOSING (BRANCH 9) (PLOT OPTION NO. 1)
134       LINE 5 - 030. TO 200.
135       LINE 32 = 1 TO 0 (CC 20)
136       LINE 35 - 0 TO 9 (CC 5)
137
138  BLOWER SPEED REDUCED & DAMPER CLOSING (PLOT OPTION NO. 1)
139       LINE 5 - 030. TO 200.
140       LINE 32 = 1 TO 0 (CC 20)
141       LINE 35 - 0 TO 9 (CC 5)
142       LINE 38 - 0 TO 2 (CC 5)
143
144  MATERIAL TRANSPORT (PLOT OPTION NO. 3)
145       LINE 5 - 030. TO 200.
146       LINE 5 - 0    0    0 TO 1    0    0
147       LINE 32 = 1 TO 0 (CC 20)
148       LINE 26 - 0 TO 1 (CC 75)
149       LINE 55 - 0 TO 1 (CC 40)
150
151  FILTER PLUGGING (PLOT OPTION NO. 3)
152       LINE 5 - 030. TO 200.
153       LINE 5 - 0    0    0 TO 1    0    0
154       LINE 26 - 0 TO 1 (CC 75)
155       LINE 32 - 1 TO 0 (CC 20)
156       LINE 55 - 0 TO 1 (CC 40)
157       LINE 61 - 0.0 TO 30.
158
```

Fig. 5.
Built-in TORAC input file (cont).

can be injected into any room or can be aerodynamically entrained and transported to the boundaries by the flow. Aerosol depletion by sedimentation will be calculated for ducts and rooms where specified. Filter plugging will occur if the filter model used is assigned a plugging coefficient.

Problem No. 1 - Tornado at Exhaust

A pressure-time function dropping to a -25 in. w.g. (about 1 psi or 6200 Pa) is placed at the exhaust boundary, node No. 10 (Figs. 6--10).

Problem No. 2 - Tornado at Intake

The same pressure-time function used in Problem No. 1 is reassigned to the system intake boundary, node No. 1 (Figs. 11--15).

Problem 3 - Material Transport (No Filter Plugging)

Problem 3 involves the transport of material injected into the room at node 4 and carried downstream by the normal operating flow of 1000 cfm. Most of this material is trapped on the filter (Figs. 16--19).

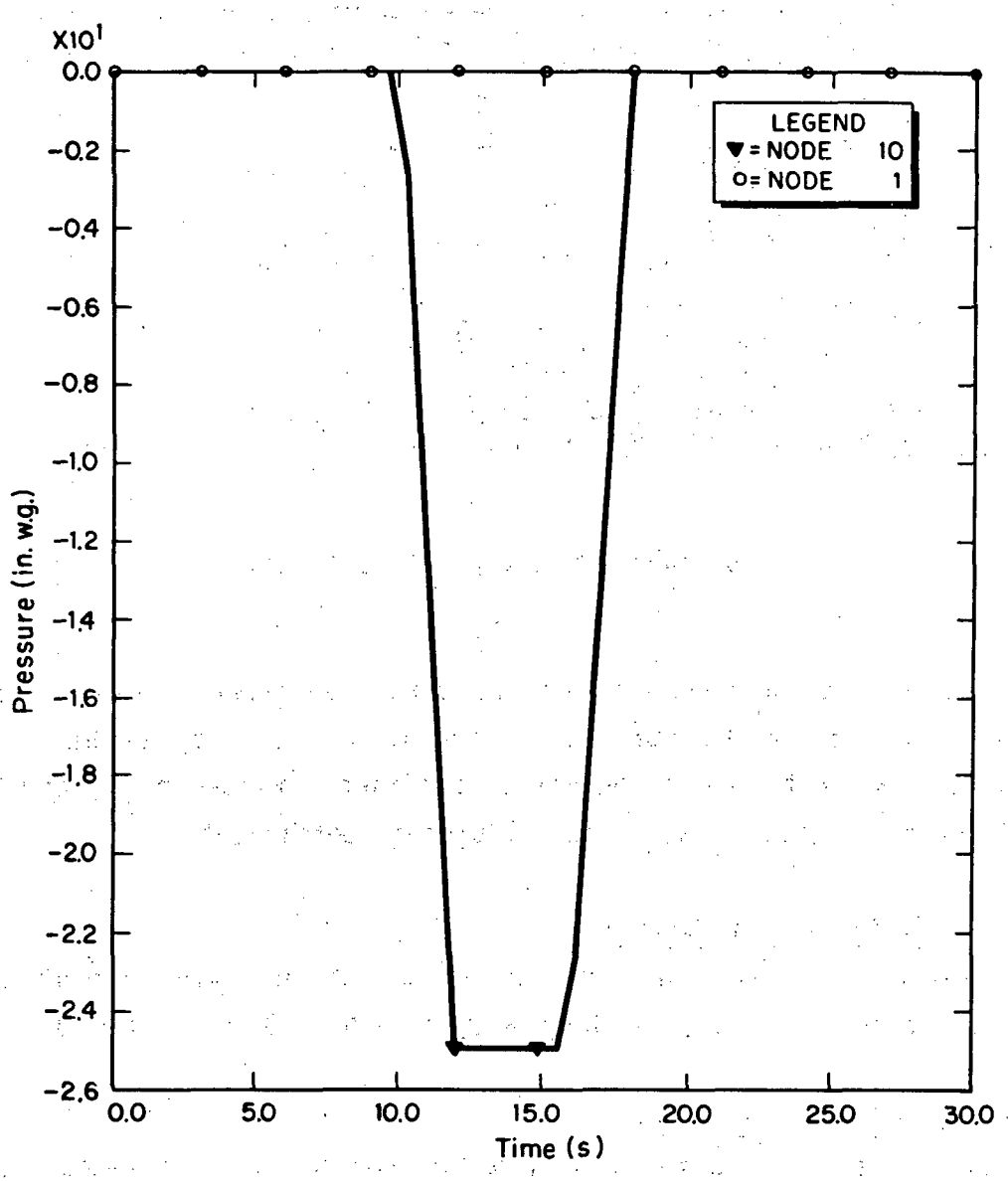

Fig. 6.
Tornado at exhaust.

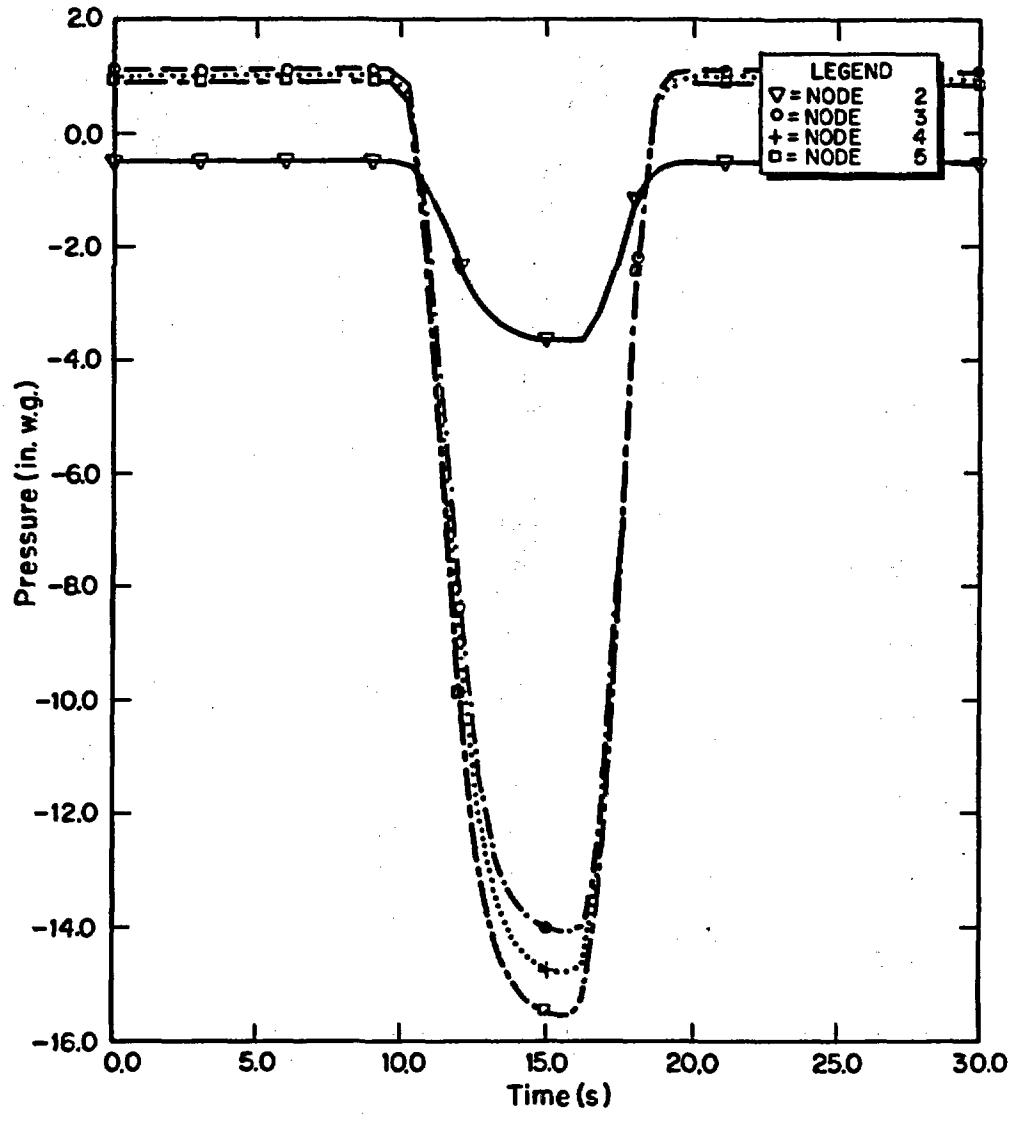

Fig. 7.
Tornado at exhaust.

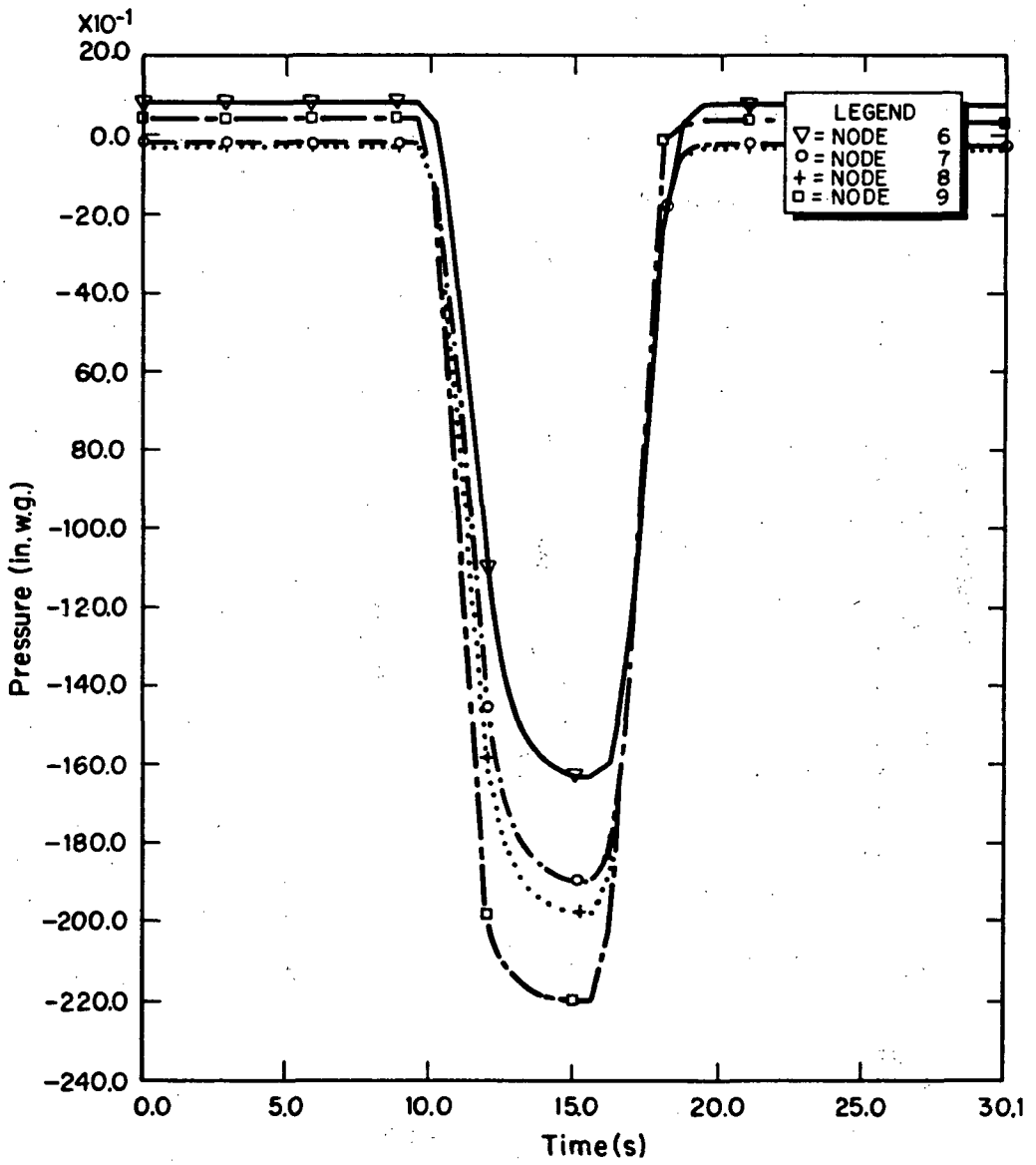

Fig. 8.
Tornado at exhaust.

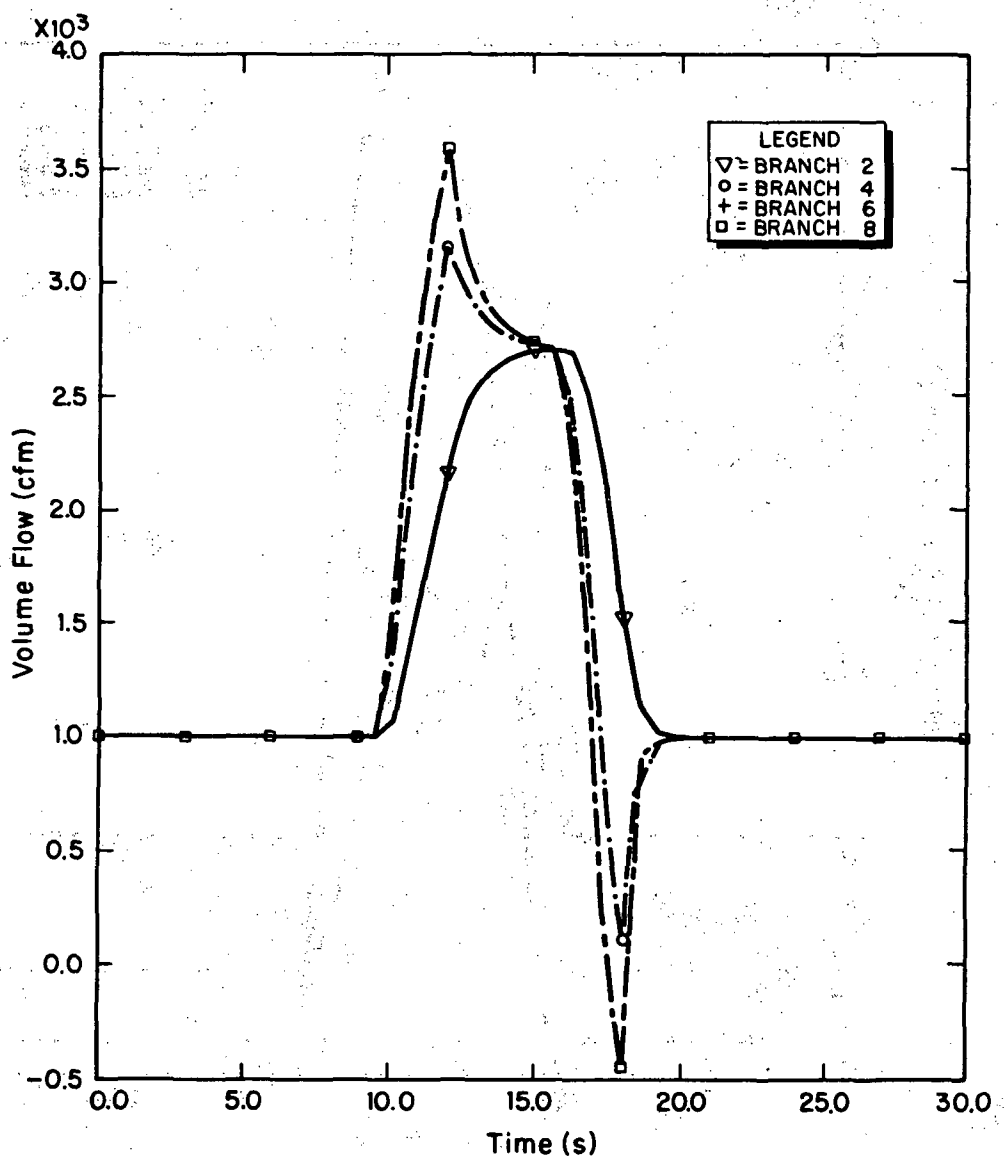

Fig. 9.
Tornado at exhaust.

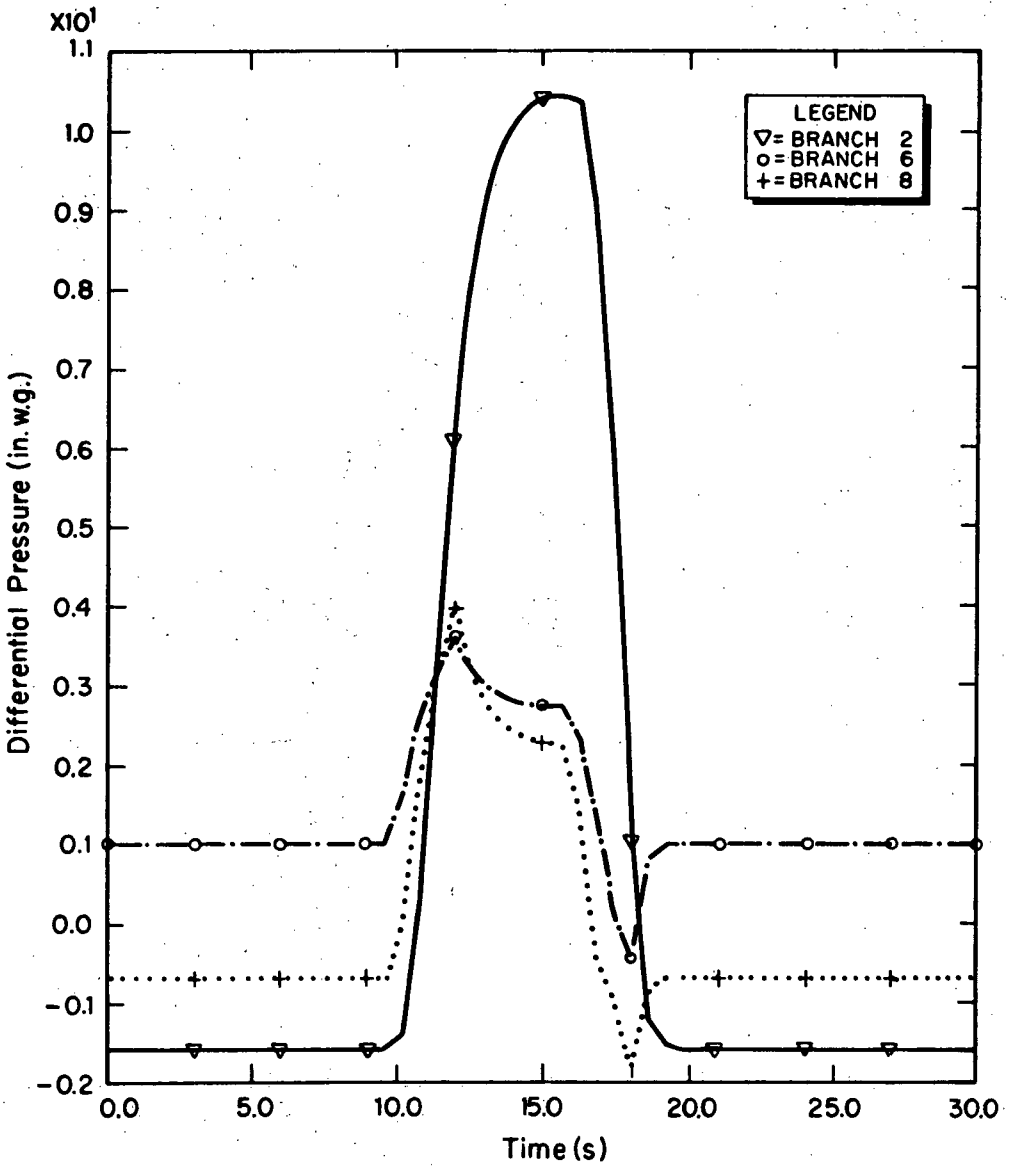

Fig. 10.
Tornado at exhaust.

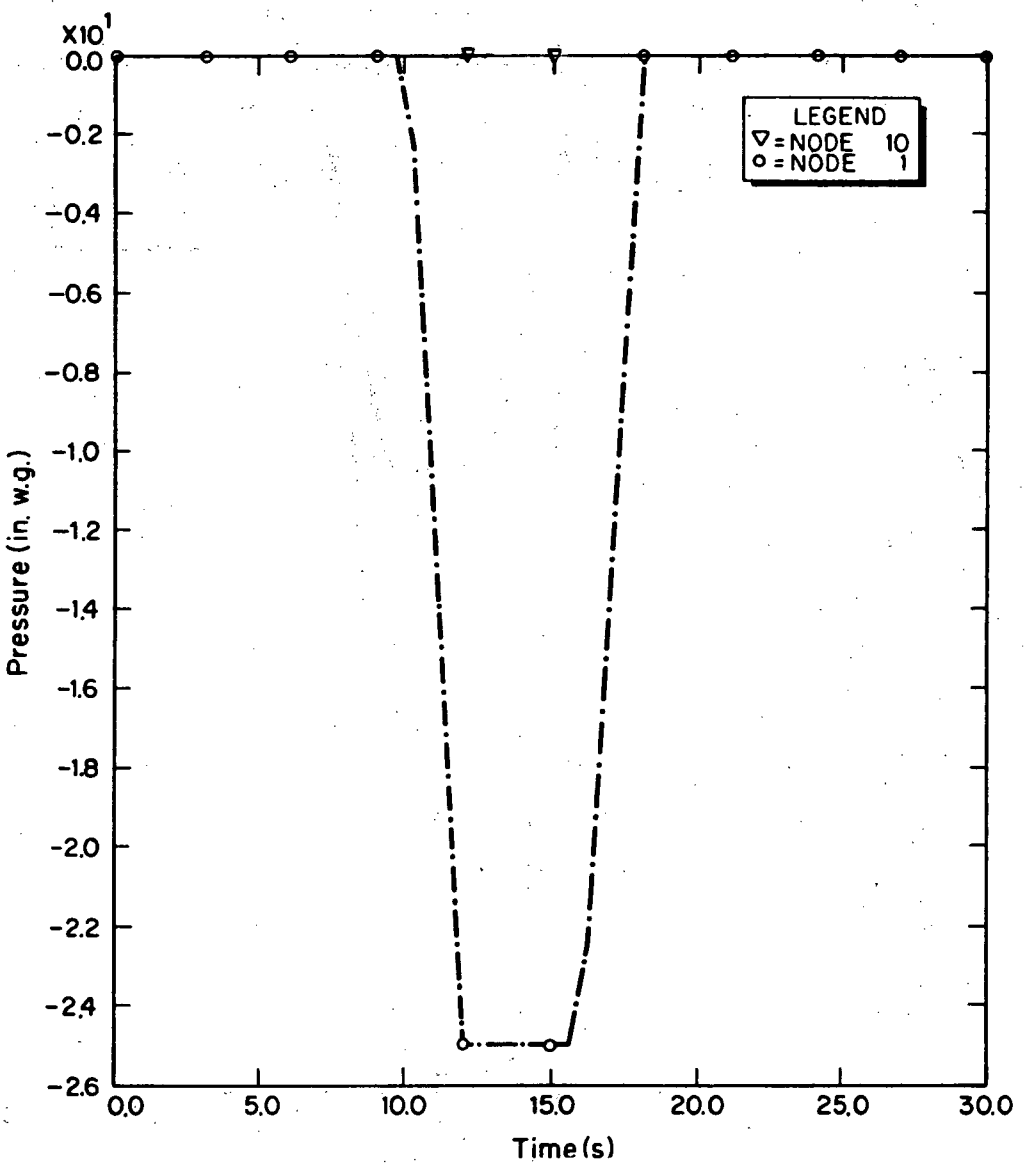

Fig. 11.
Tornado at intake.

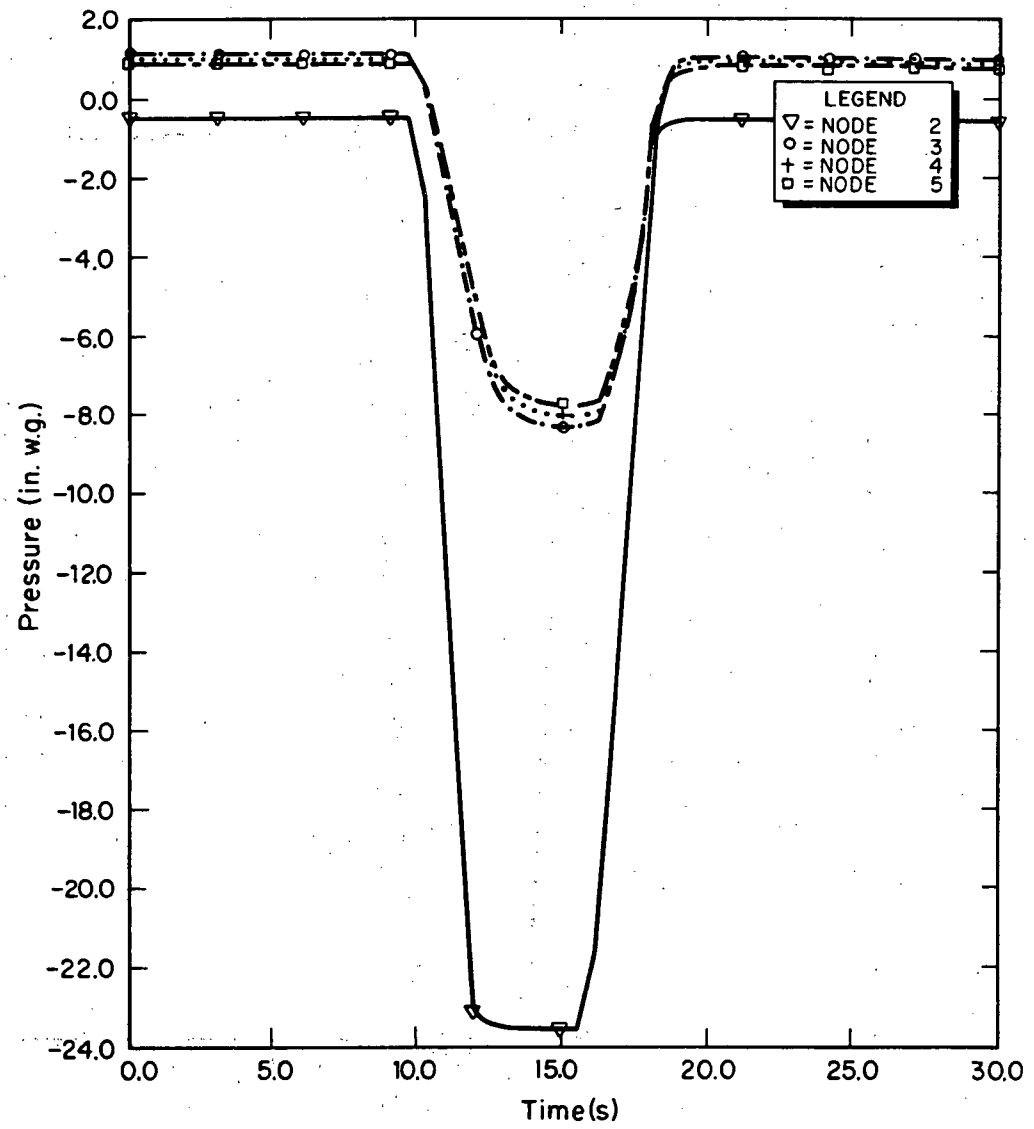

Fig. 12.
Tornado at intake.

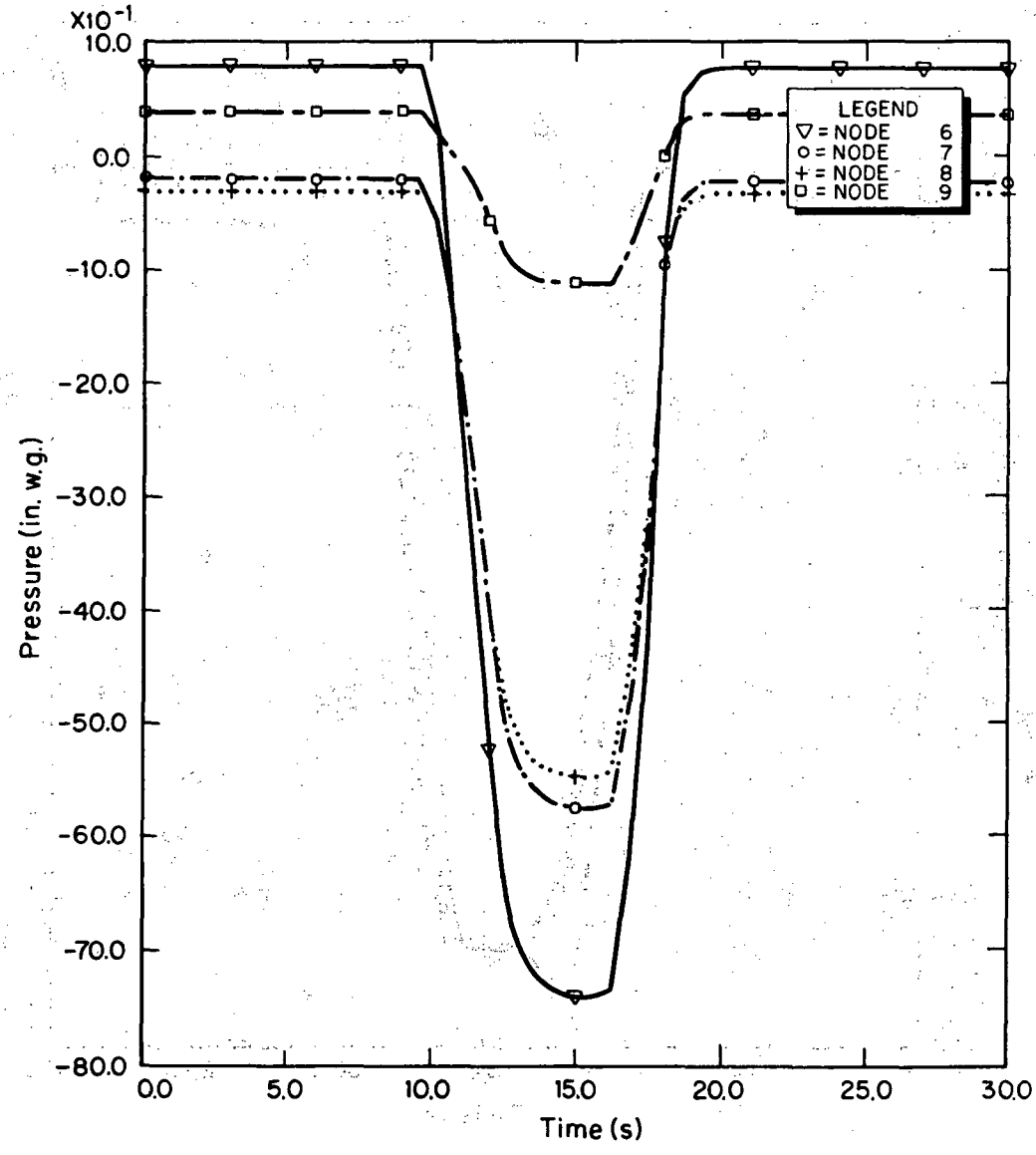

Fig. 13.
Tornado at intake.

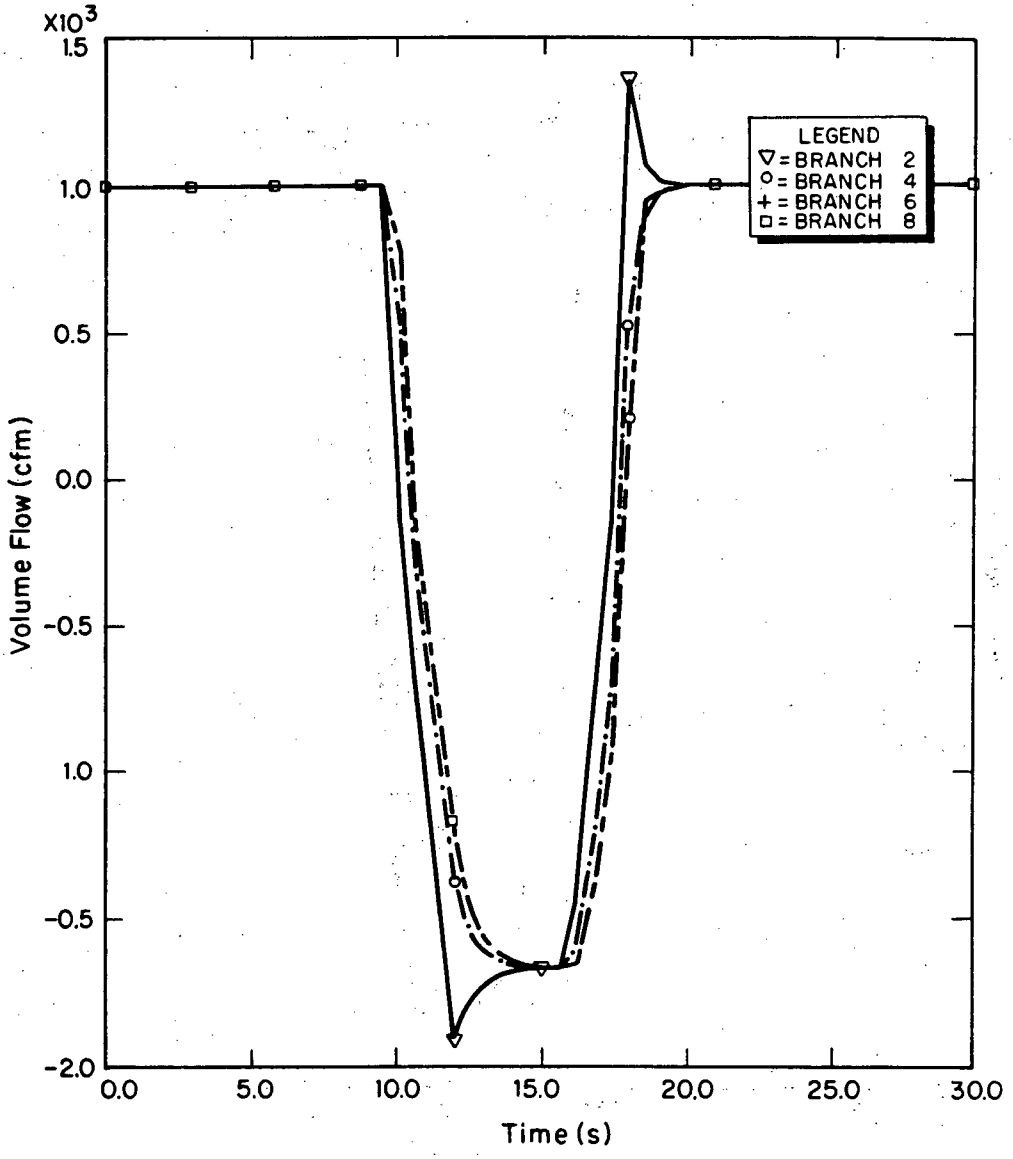

Fig. 14.
Tornado at intake.

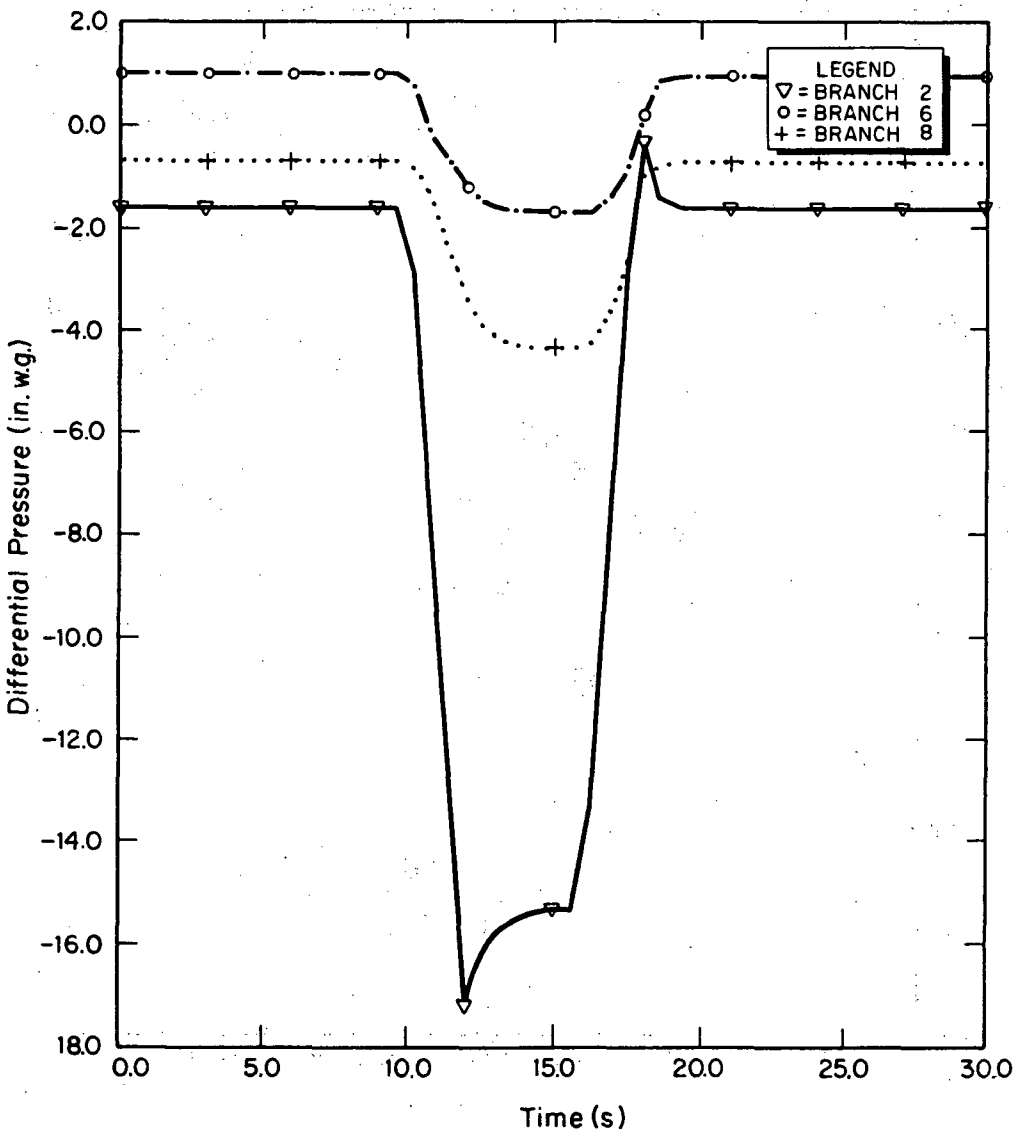

Fig. 15.
Tornado at intake.

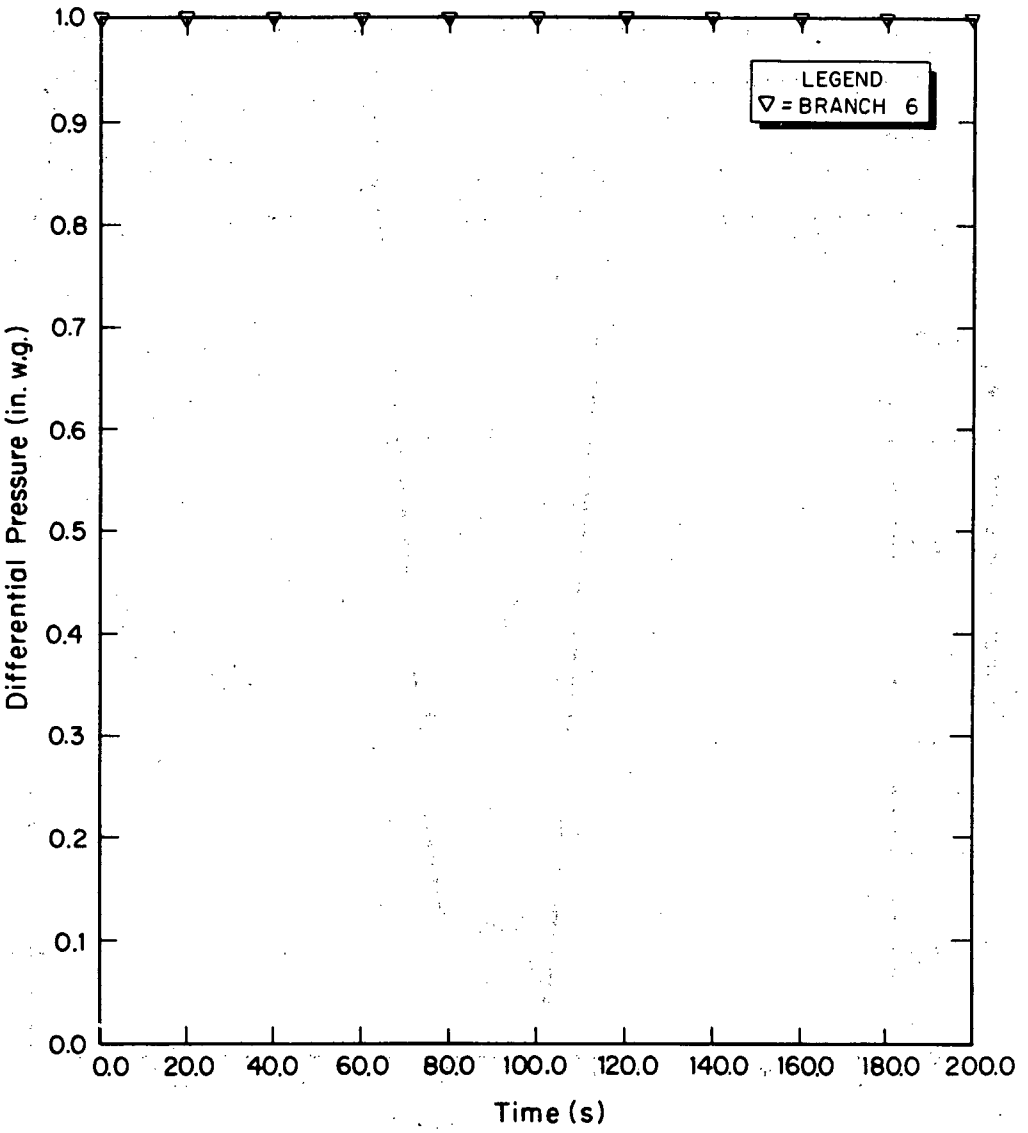

Fig. 16.
Material transport (no filter plugging).

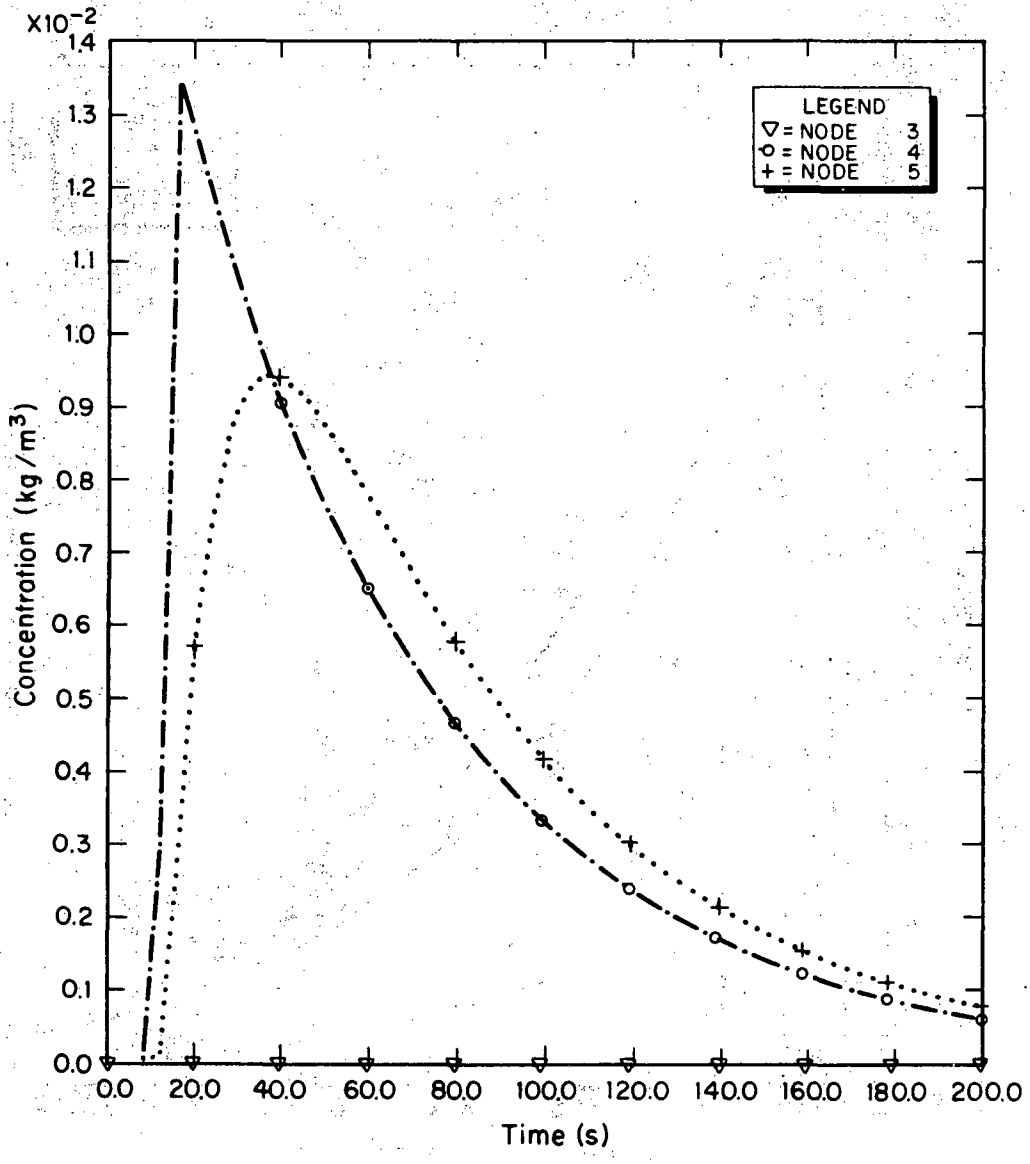

Fig. 17.
Material transport (no filter plugging).

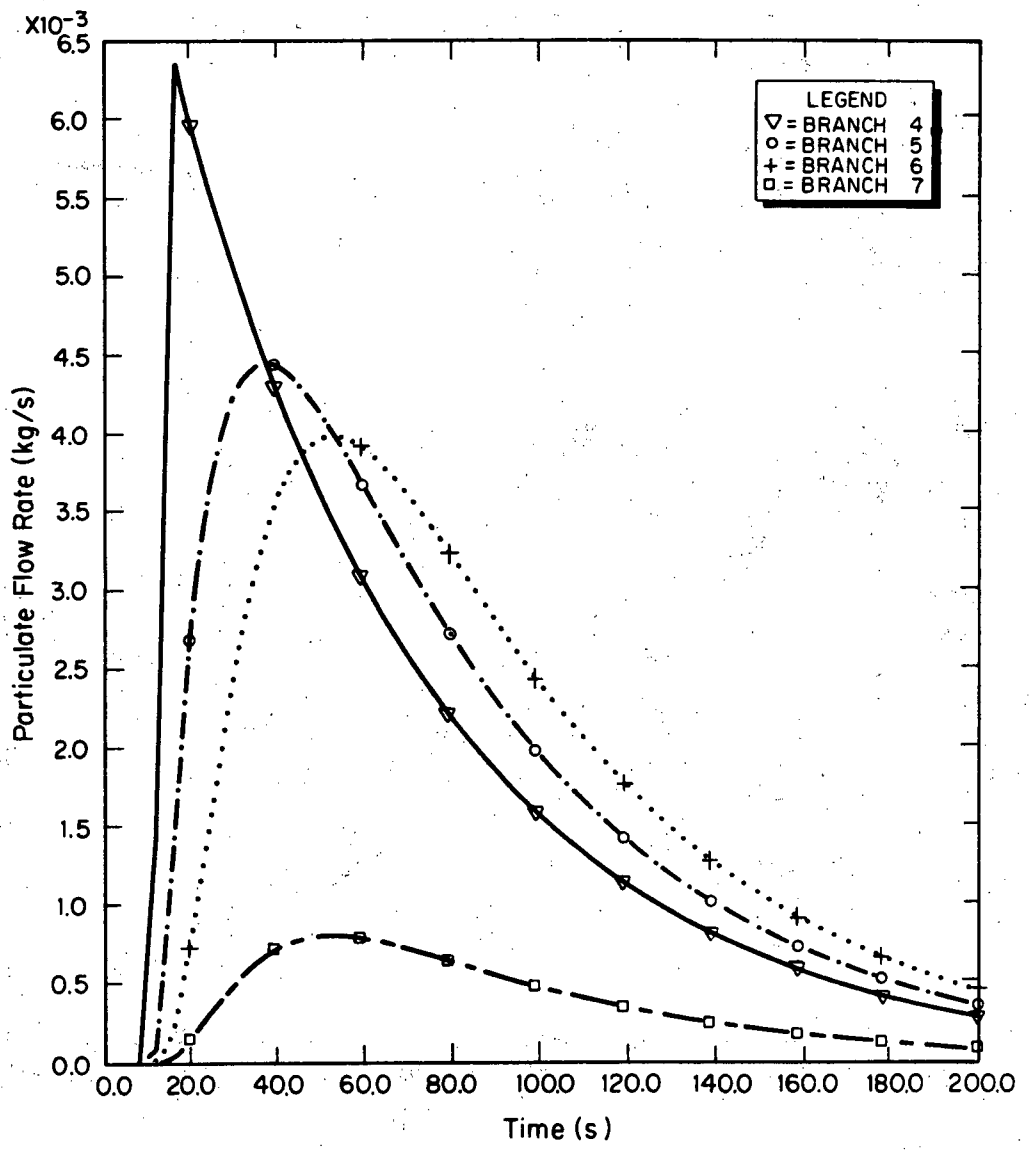

Fig. 18.
Material transport (no filter plugging).

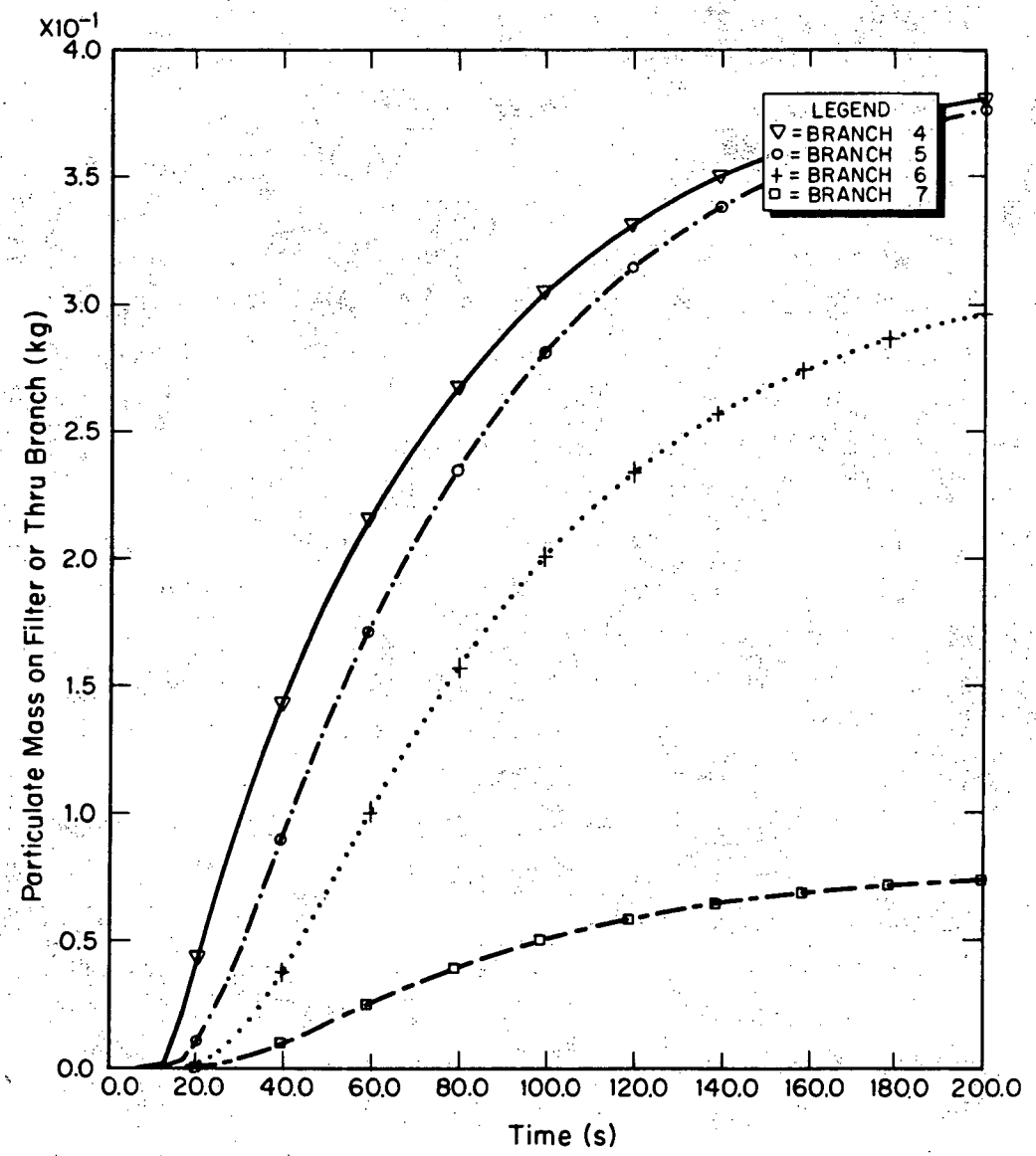

Fig. 19.
Material transport (no filter plugging).

Problem 4 - Material Transport (Filter Plugging)

Problem 4 also involves the transport of material injected into the room at node 4 and carried downstream by the normal operating flow of 1000 cfm. This is the same condition as in problem No. 6, but the filter has been assigned a plugging factor of 30 (Figs. 20--23.)

Problem 5 - Calculated Aerodynamic Entrainment

This sample problem illustrates the use of the calculated aerodynamic entrainment option for material transport initiation in a duct. The user requirements and theory for this option are discussed above. For convenience, we used the same system shown in Figs. 3 and 4. The 100-ft-long duct connecting the room at node 4 to the filter in branch 6 was modeled using two segments. Each segment contained a resistance lumped in a branch and a volume lumped at a node. Duct entrainment should be specified at the latter nodes. For more accurate results, more segments should be used. In this version of TORAC, entrainment of beds of material in rooms or cells is treated in the same way as illustrated here. The following conditions were assumed and set up in the master input file of TORAC. (See Fig. 5.)

1. Tornado of strength 50 in. w.g. simulated at exhaust node 10.
2. No material injection (transport initiation) in room 4 or elsewhere using the user-specified option.
3. A total of 1 kg of contaminant material is subjected to entrainment in the duct volume represented by node 5.
4. The contaminant material is assumed to consist of homogeneous, monodisperse, spherical particles with aerodynamic diameter D_p = 100 μm (10^{-4}m) and bulk density ρ_p = 3 g/cm^3 (3000 kg/m^3).
5. The contaminant material is distributed uniformly over the 2- by 50-ft floor area of duct volume 5.
6. No deposition occurs in duct branches 4 or 5. (The volumes of these branches were modeled by nodes 5 and 6, respectively.)
7. The filter efficiency was set at 0.8.

Our choice of material and surface loading for this example was somewhat arbitrary. Specific values are presented for illustrative purposes only. Based on data for mixed-oxide fuel (PuO_2 powder size),[1,16] a more realistic choice may be mass median aerodynamic diameter equals 20 μm and density equals 10 g/cm^3. The

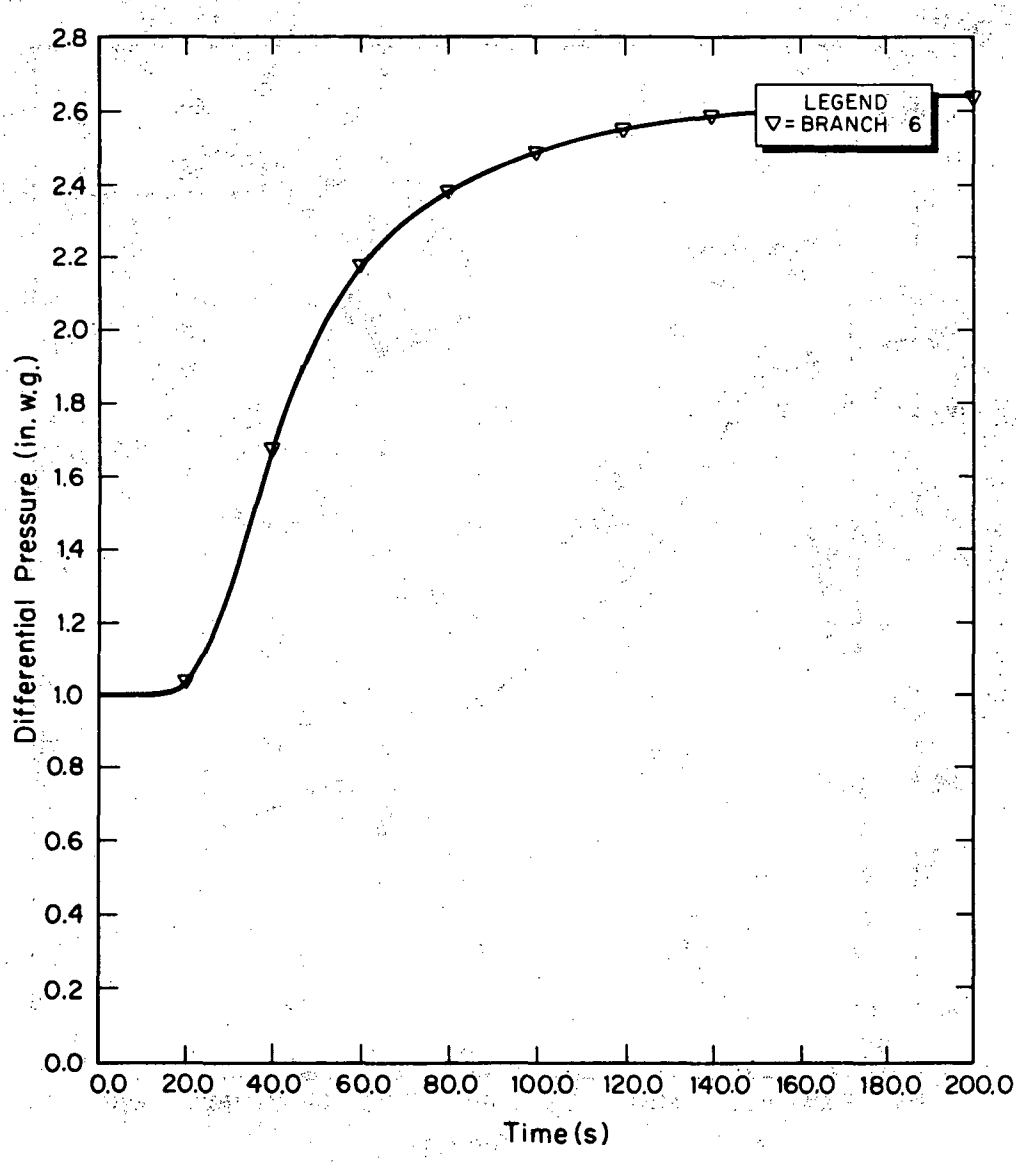

Fig. 20.
Material transport (filter plugging).

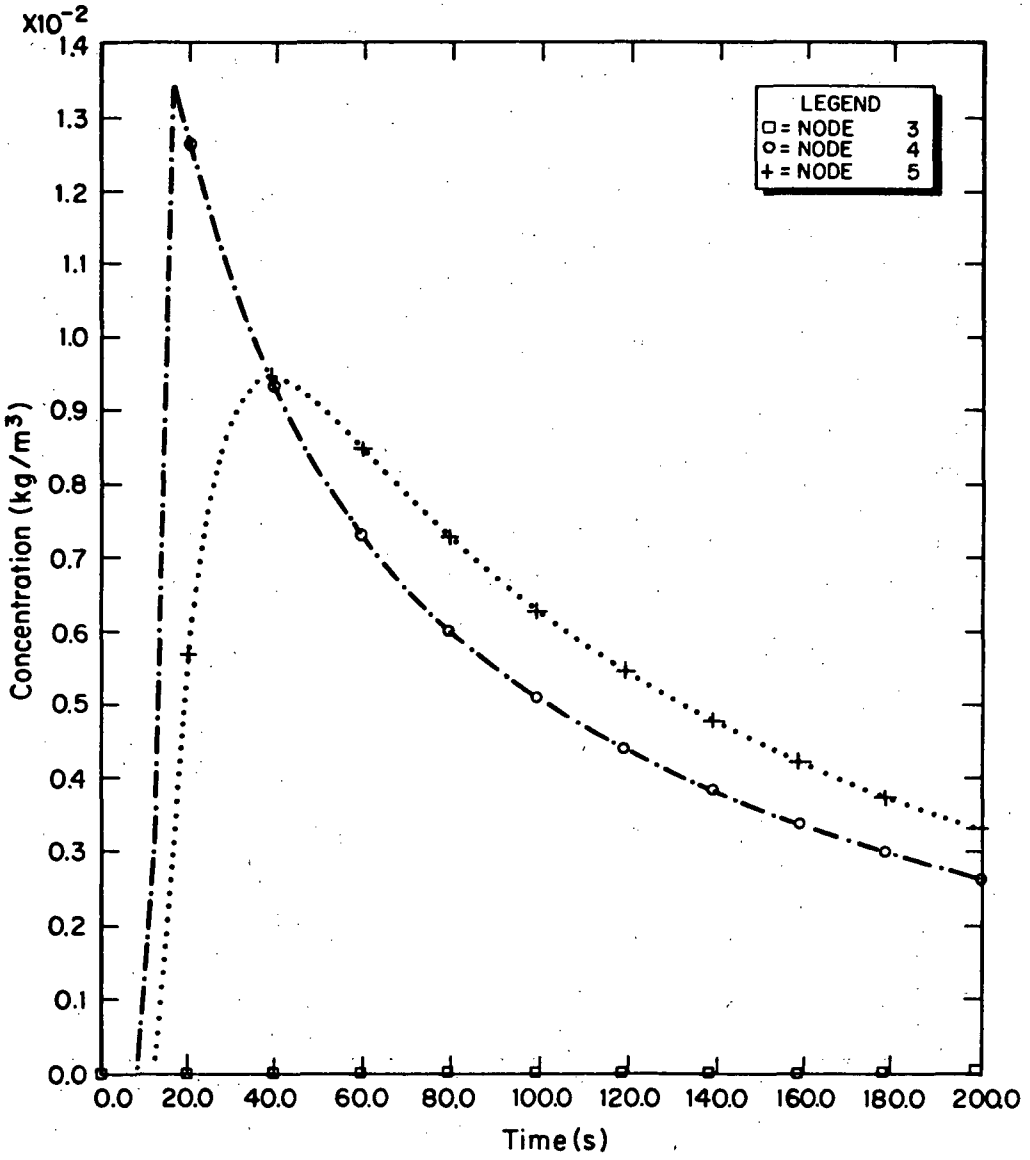

Fig. 21.
Material transport (filter plugging).

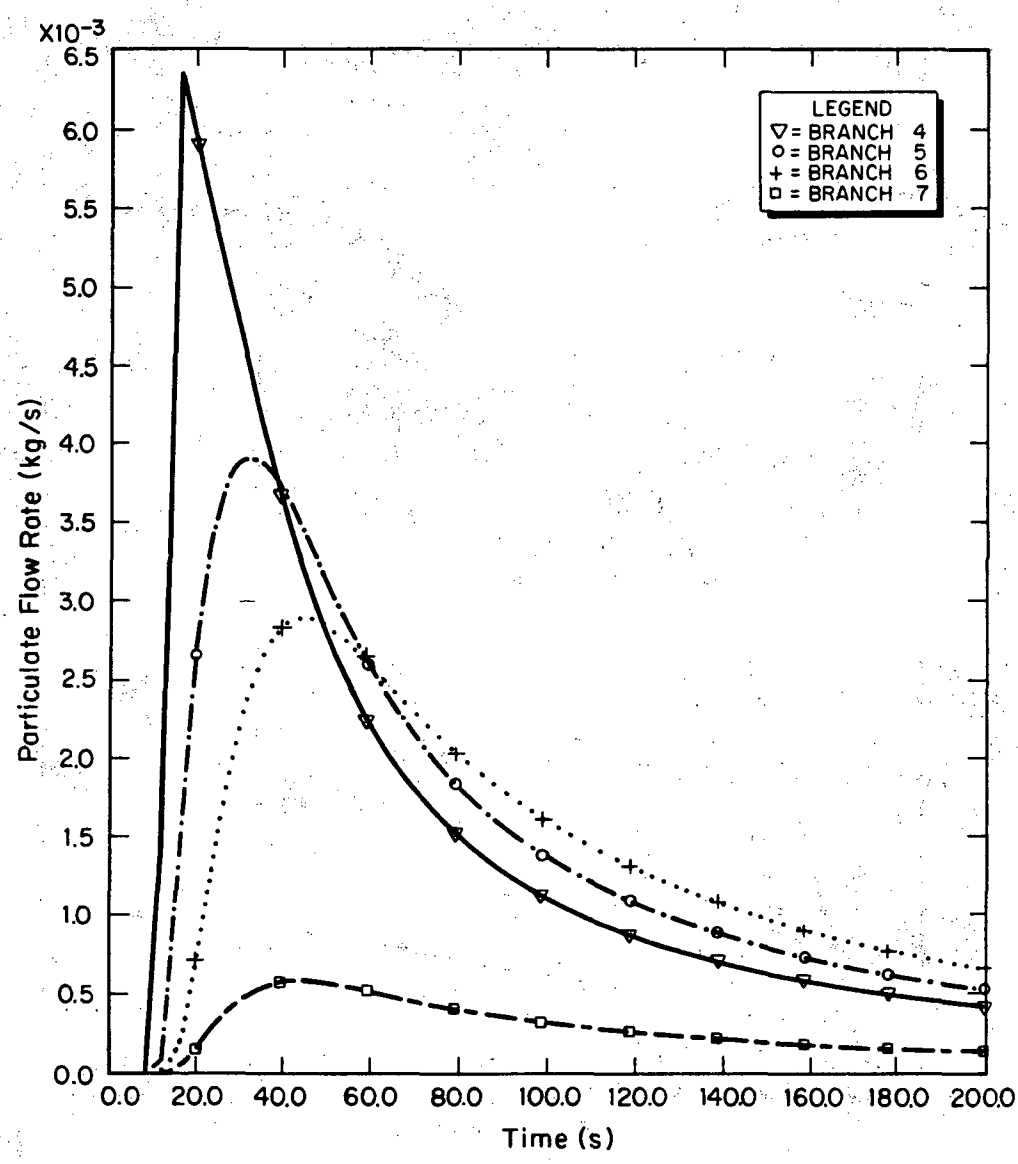

Fig. 22.
Material transport (filter plugging).

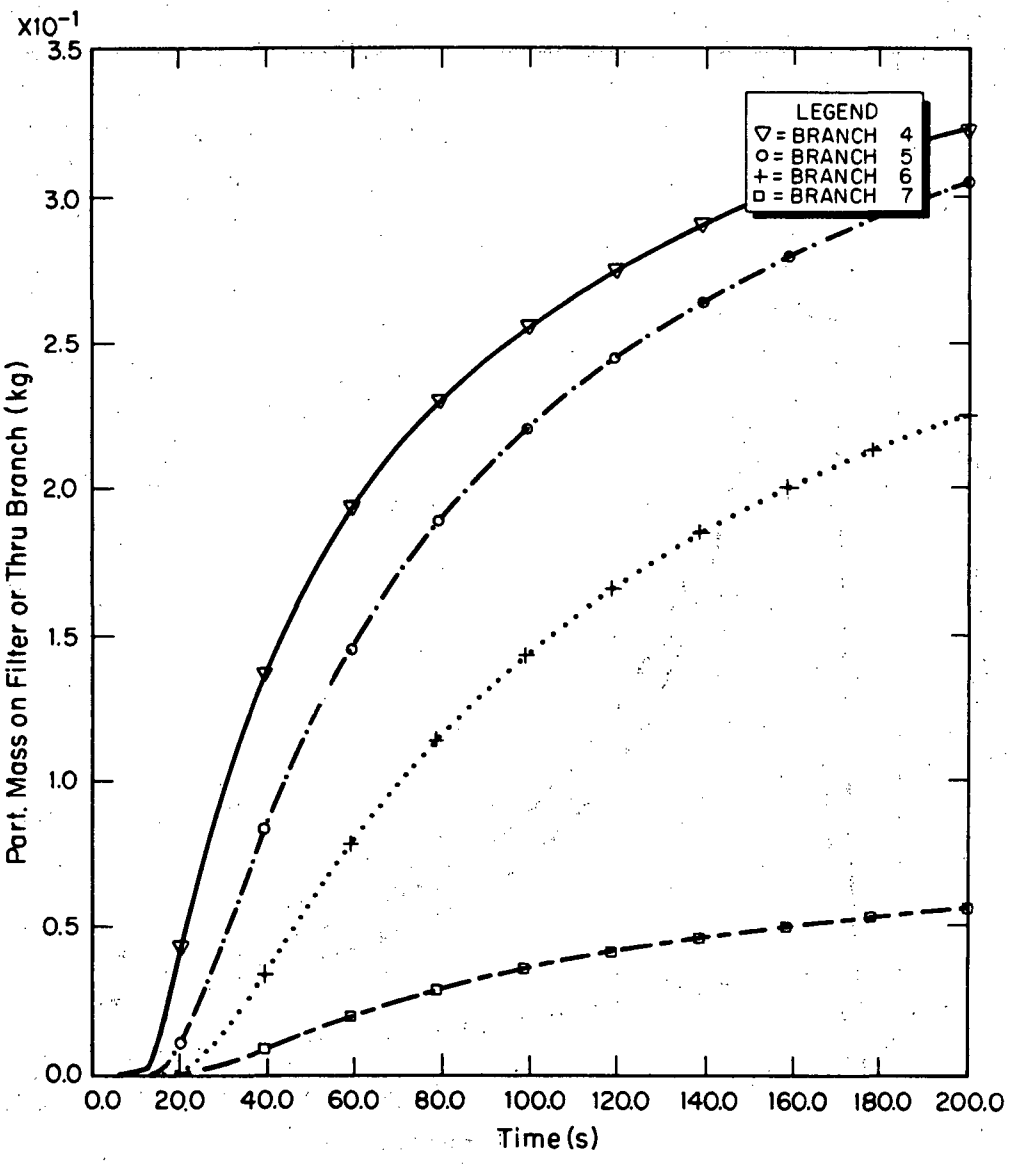

Fig. 23.
Material transport (filter plugging).

theoretical density of PuO_2 is about 11.5 g/cm^3. The values used here may be representative of a more agglomerated material. The material loading of 27 g/m^2 (based on four surfaces) for duct volume 5 is about four times the loading of 7 g/m^2 for a very dusty surface. The latter material loading value is discussed in Ref. 1.

The tornado-induced nodal pressure time histories for this example are similar in shape to those shown in Figs. 6—8 except that they show more negative peaks in gauge pressure because the tornado is more severe in the current example. The peak negative gauge pressure for node 10 is -50 in. w.g. compared with -25 in. w.g., which was shown in Fig. 6. On these figures, the symbols T(50) and D(100) refer to the tornado strength of 50 in. w.g. and the particulate diameter of 100 μm, respectively.

The results of sample Problem 5 are shown in Figs. 24—27. The volume flow rates in four selected branches are shown in Fig. 24. These flows were induced by a tornado depressurization from 0 to -50 in. w.g. pressure between times 10 and 12 s, constant at -50 in. w.g. pressure from times 12 s to 16 s, and back up to 0 in. w.g. pressure at time 18 s. A flow reversal occurs in branches 4, 5, and 8 at about 18 s. The material concentration time histories for four selected nodes are shown in Fig. 25. Aerodynamic entrainment of powder with D_p = 100 μm and ρ_p = 3 g/cm^3 from thick beds may be expected for surface friction velocities exceeding a threshold value of about u_{*t} = 21.7 cm/s. This corresponds to an air velocity of about U = 374 cm/s (12.3 ft/s) and an airflow rate of about Q = 3000 ft^3/min through a duct with a cross section of 4 ft^2. In Fig. 24 for branch 4, Q = 3000 ft^3/min is induced by the tornado at about t = 12 s. At about this time, the aerosol concentration at node 5 jumps as a spike to over 0.16 kg/m^3 (Fig. 25). If 1 kg of material were injected instantly into the 200 ft^3 volume of the duct segment represented by node 5, we would expect an instantaneous spike in concentration to 0.18 kg/m^3. The airborne material is convected into node 6 and partially collected on the 80% filter in branch 6. The particulate flow rate is shown in Fig. 26. Figure 27 gives the cumulative particulate mass on a filter or through each branch. The curves in Fig. 27 represent the integral of their counterparts in Fig. 26. At t = 30 s in this example, Fig. 27 shows that about 0.92 kg of material was removed from node 5 with about 0.15 kg surviving the filter. The net reduction in concentration ahead of the filter observed here is caused by dilution and time delay only as deposition was turned off. That is, before material can flow through

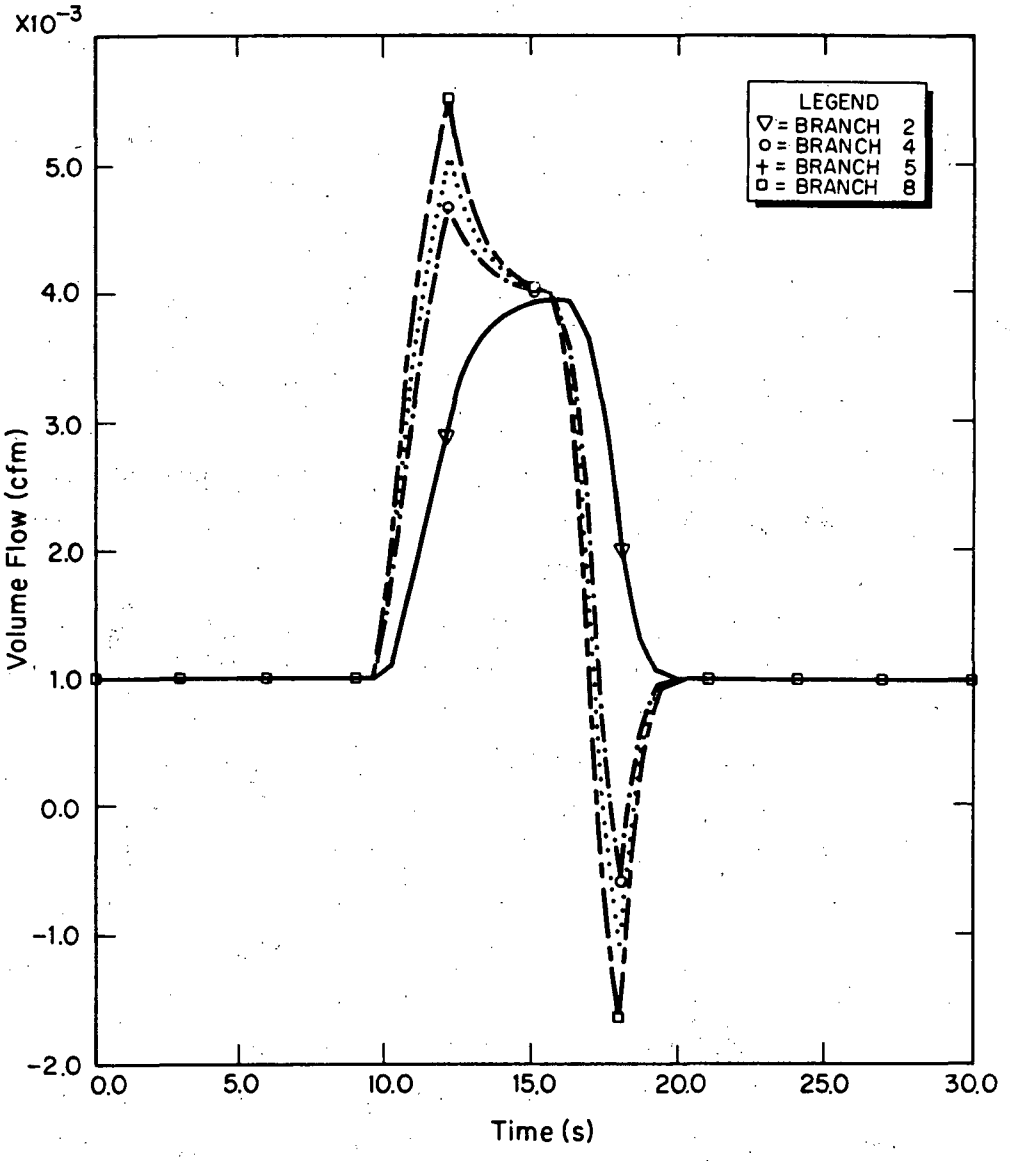

Fig. 24.
Entrainment: T(50), D(100).

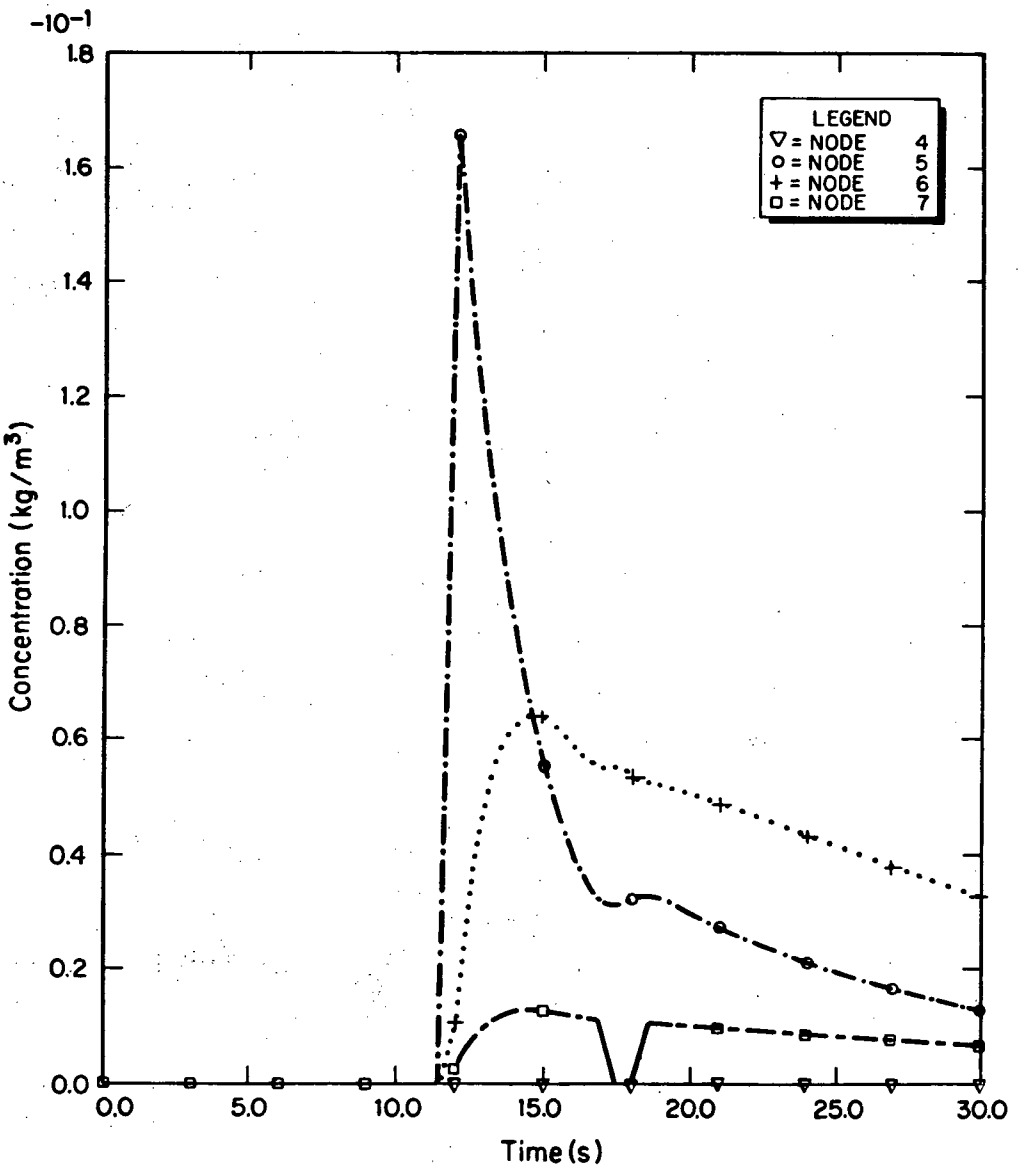

Fig. 25.
Entrainment: T(50), D(100).

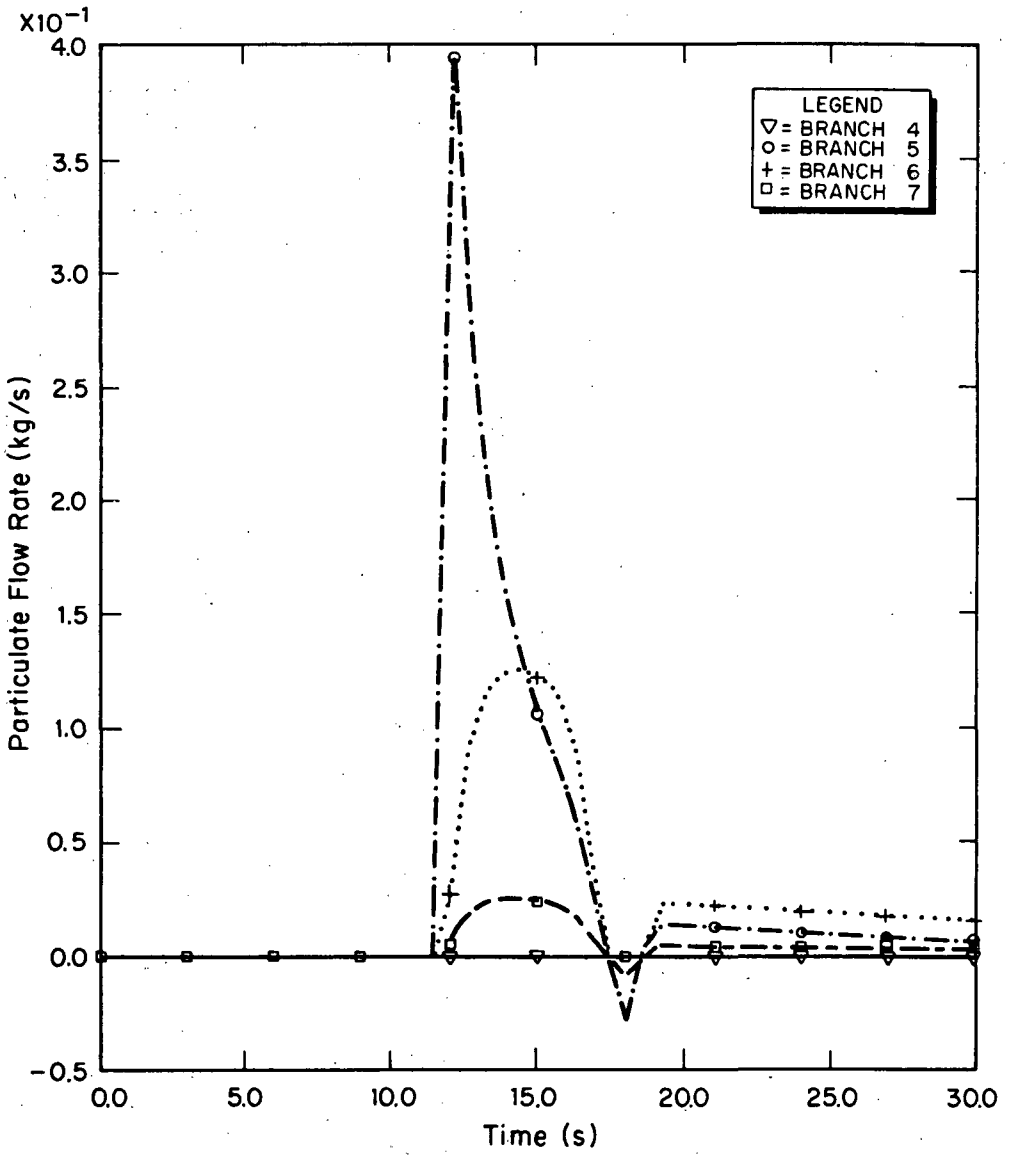

Fig. 26.
Entrainment: T(50), D(100).

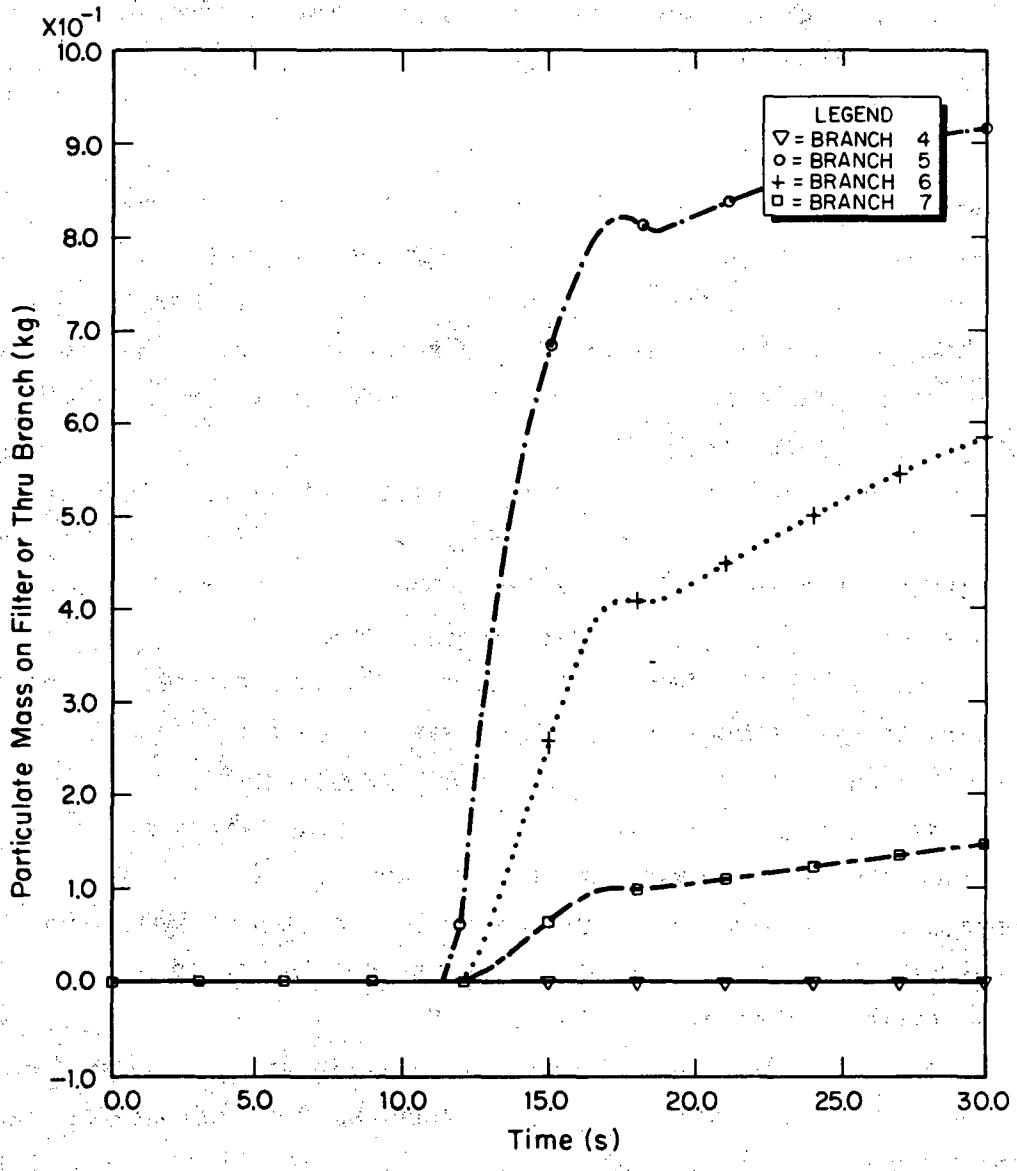

Fig. 27.
Entrainment: T(50), D(100).

branch 6 (filter), the concentration in node 6 (duct volume) must be built up by material flow in branch 5 following entrainment in node 5. Deposition by sedimentation was turned off in this example for simplicity and clarity but could have been turned on simultaneously with entrainment. Problem 6 shows that this 100-μm, 3-g/cm^3 material would have been substantially removed from suspension if the deposition module had been turned on.

Problem 6 - Aerosol Depletion

This problem illustrates TORAC's capability to account for aerosol depletion by gravitational sedimentation. The user requirements and theory for this subroutine are discussed above. As before, our model is shown schematically in Figs. 3 and 4. In this version of TORAC, aerosol depletion is handled in the same way for ducts and rooms. The following conditions were assumed and set up in the TORAC master input (Fig. 5).

1. Tornado of strength 50 in. w.g. simulated at exhaust node 10.
2. From times t = 10 s to t = 16 s, a total of 0.4 kg of aerosol is injected into the 1000-ft^3-volume room represented by node 4.
3. No material is subject to entrainment anywhere.
4. The contaminant material is assumed to be composed of homogeneous, monodisperse, spherical particles with aerodynamic diameter D_p = 10 μm (10^{-5}m) and bulk density ρ_p = 3 g/cm^3 (3000 kg/m^2).
5. As the contaminant material is injected, it instantly forms a homogeneous mixture with the air in room 4.
6. Deposition by sedimentation occurs in the duct lengths represented by volumes at nodes 5 and 6 only (and was not turned on for room 4).
7. The filter efficiency was set at 0.8.

In this example we illustrate the alternate user-input option for material transport initiation as opposed to the other option, calculated aerodynamic entrainment, which was illustrated in Problem 5. Material is injected at node 4 to simulate accident conditions there. Deposition occurs in the two downstream duct segments. The choice of material characteristics for this example is strictly hypothetical and different from that discussed for Problem 5. (See example Problem 5 above.) The same tornado pressure function described in Problem 5 was used here. However, the material generation function goes from 0 kg/s at time t = 10 s to 0.1 kg/s at t = 12 s, stays constant until t = 14 s, and returns to 0 kg/s at t = 16 s. (See Fig. 5.)

The results of sample Problem 6 are shown in Fig. 24 and Figs. 28--32. That is, the tornado-induced airflow time histories are identical to those discussed for Problem 5. The material concentration histories for four selected nodes are shown in Fig. 28. The aerosol concentration in room 4 begins to rise immediately at t = 10 s because that is when material injection begins. As the 1000-ft^3 room 4 receives aerosol, the concentration goes up and peaks at t = 16 s. Meanwhile, there is a delay while the particulate-laden air drawn out of room 4 flows into duct volume 5. The dip in the concentration profiles at about t = 17.5 s was caused by the flow reversal. Figure 29 also shows this momentary flow reversal in particulate flow rate. The material accumulations on the filter (branch 7) and passing through branches 4--6 are shown in Fig. 30. Although 0.4 kg of aerosol is injected into room 4 during $10 \leq t \leq 16$ s, the accumulated aerosol mass flow passing through branch 4 at t = 30 s is only about 0.143 kg. This is because fresh air from branch 3 is diluting the mixture in room 4 continually. By t = 120 s, the accumulation of mass through branch 4 is about 0.34 kg, and the concentration in node 4 is down to about 0.0012 kg/m^3 (not shown in Fig. 30). The effect of deposition can be observed by comparing Fig. 30 with Figs. 31 and 32. Figure 31 was run for the same conditions as Figs. 28--30 except that deposition in branches 4 and 5 was shut off. The reduction in accumulation of 10-μm material in branches 5--7 in Fig. 30 from Fig. 31 is relatively small. However, material losses resulting from sedimentation in these branches are more pronounced in Fig. 32. The results shown in Fig. 32 were obtained for the same conditions as for Figs. 28--30 except that the material size was input as 100 μm instead of 10 μm. Figure 32 should be compared with Figs. 30 and 31.

X. SUMMARY

To insure that nuclear facilities can withstand postulated accidents, regulatory agencies have the responsibility of reviewing proposed facility designs. The degree of conservatism and the related risk assessment also must be evaluated for these accident conditions. The nature of the hazardous material involved and the potential for accidents require designers and analysts to have methods and supportive experimental data for a systematic approach to estimating accident effects.

Assessment of the environmental consequences of an accident ultimately involves calculating atmospheric dispersion and radioactive dosage estimates

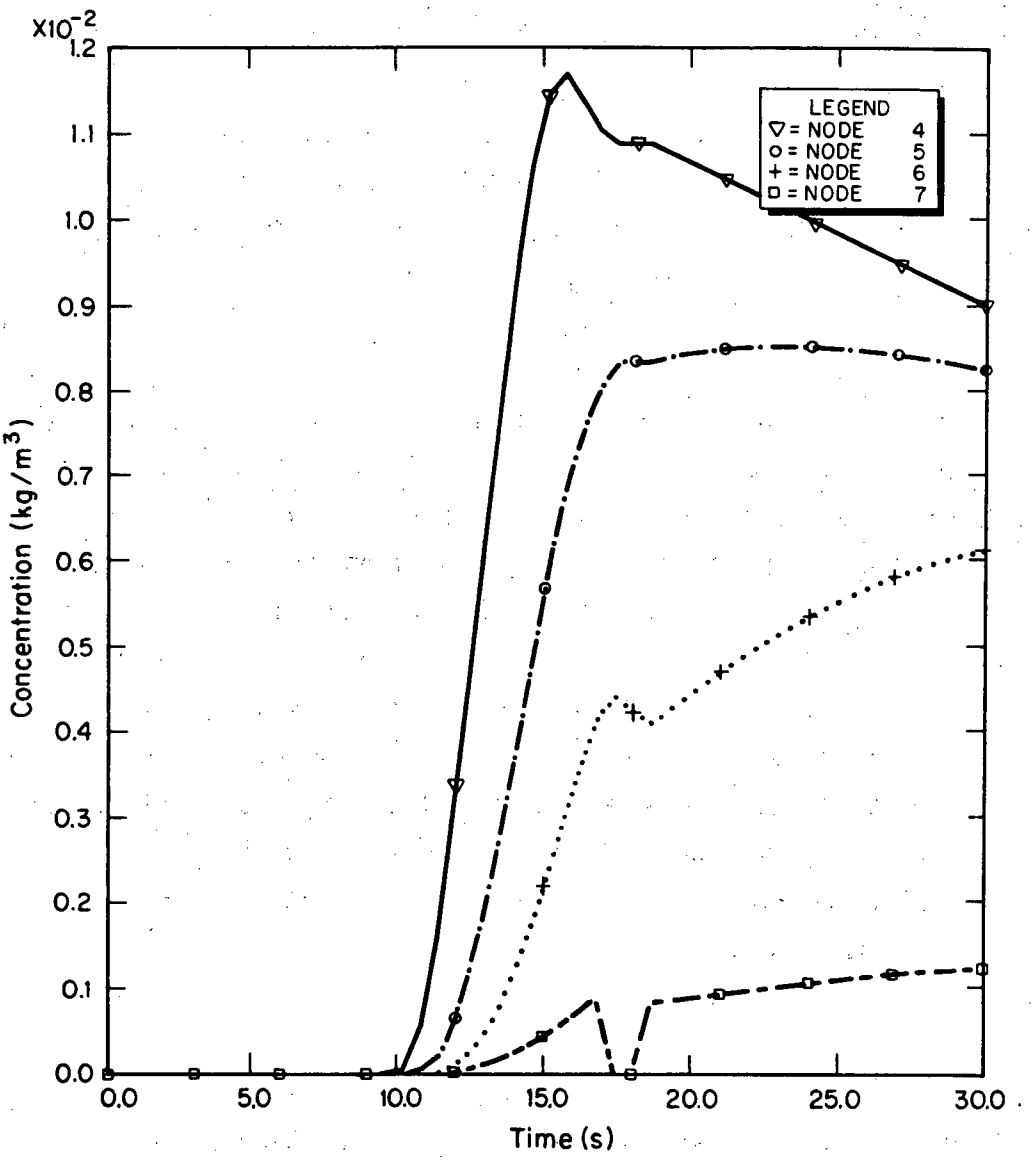

Fig. 28.
Deposition: T(50), D(10).

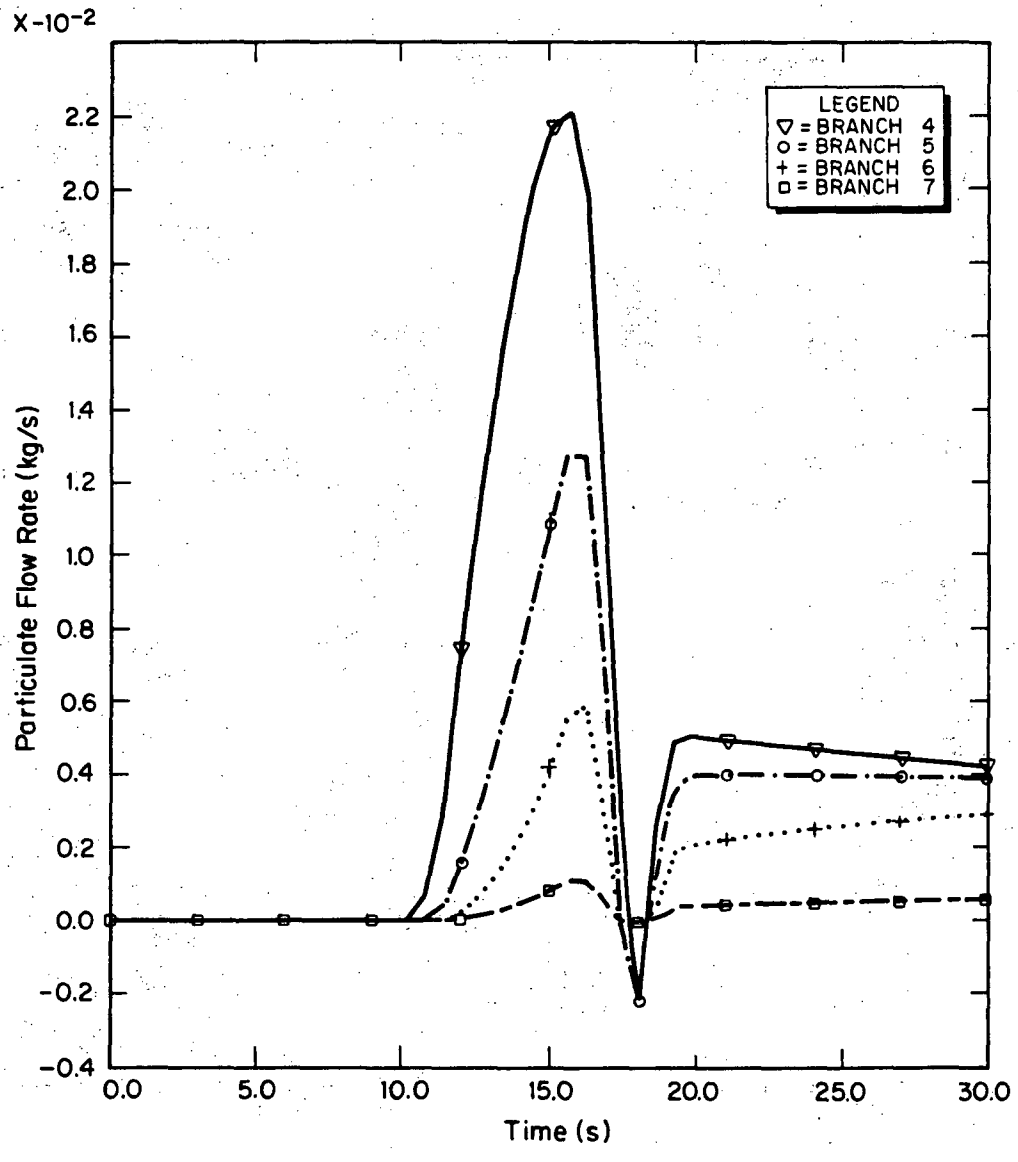

Fig. 29.
Deposition: T(50), D(10).

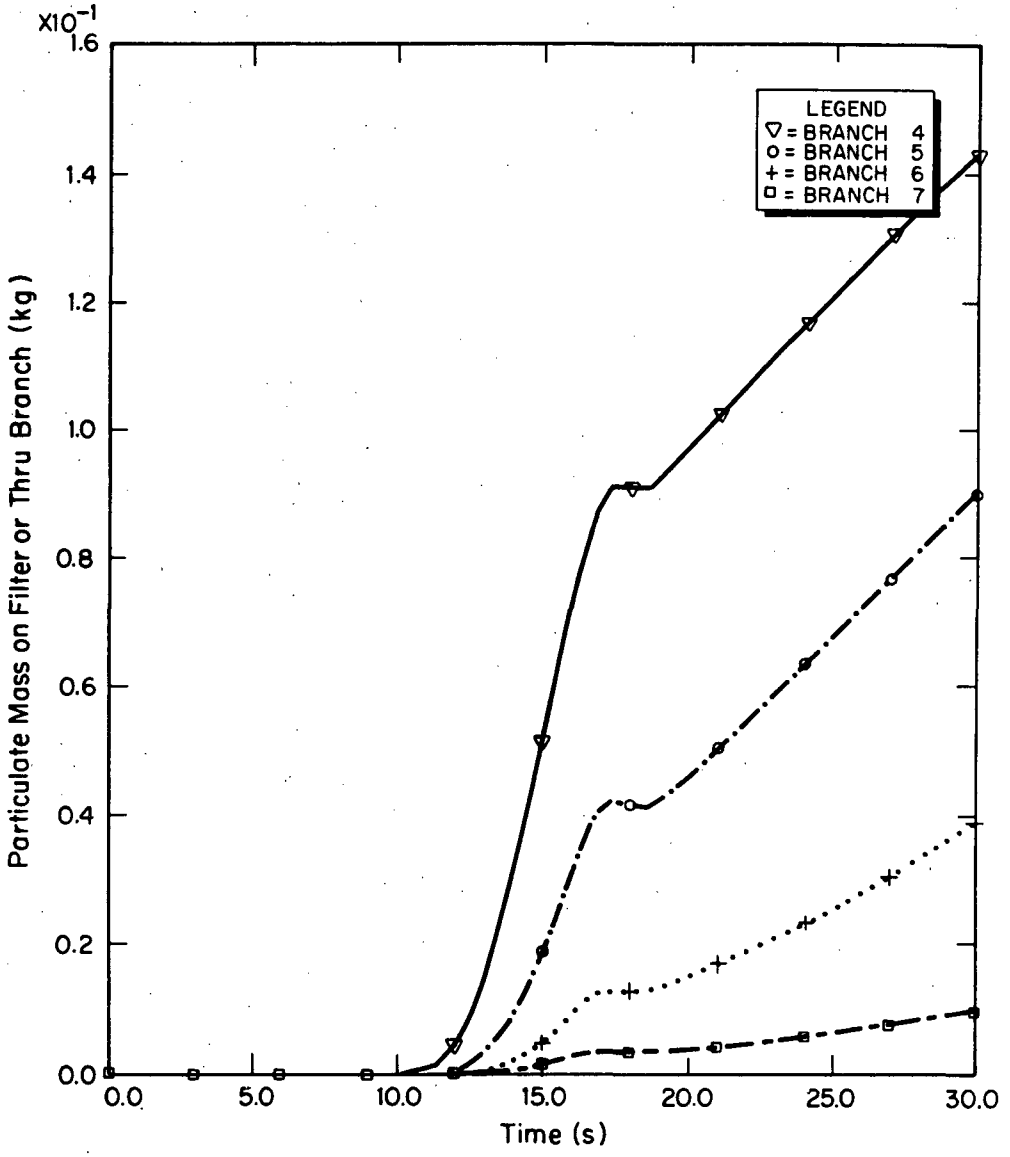

Fig. 30.
Deposition: T(50), D(10).

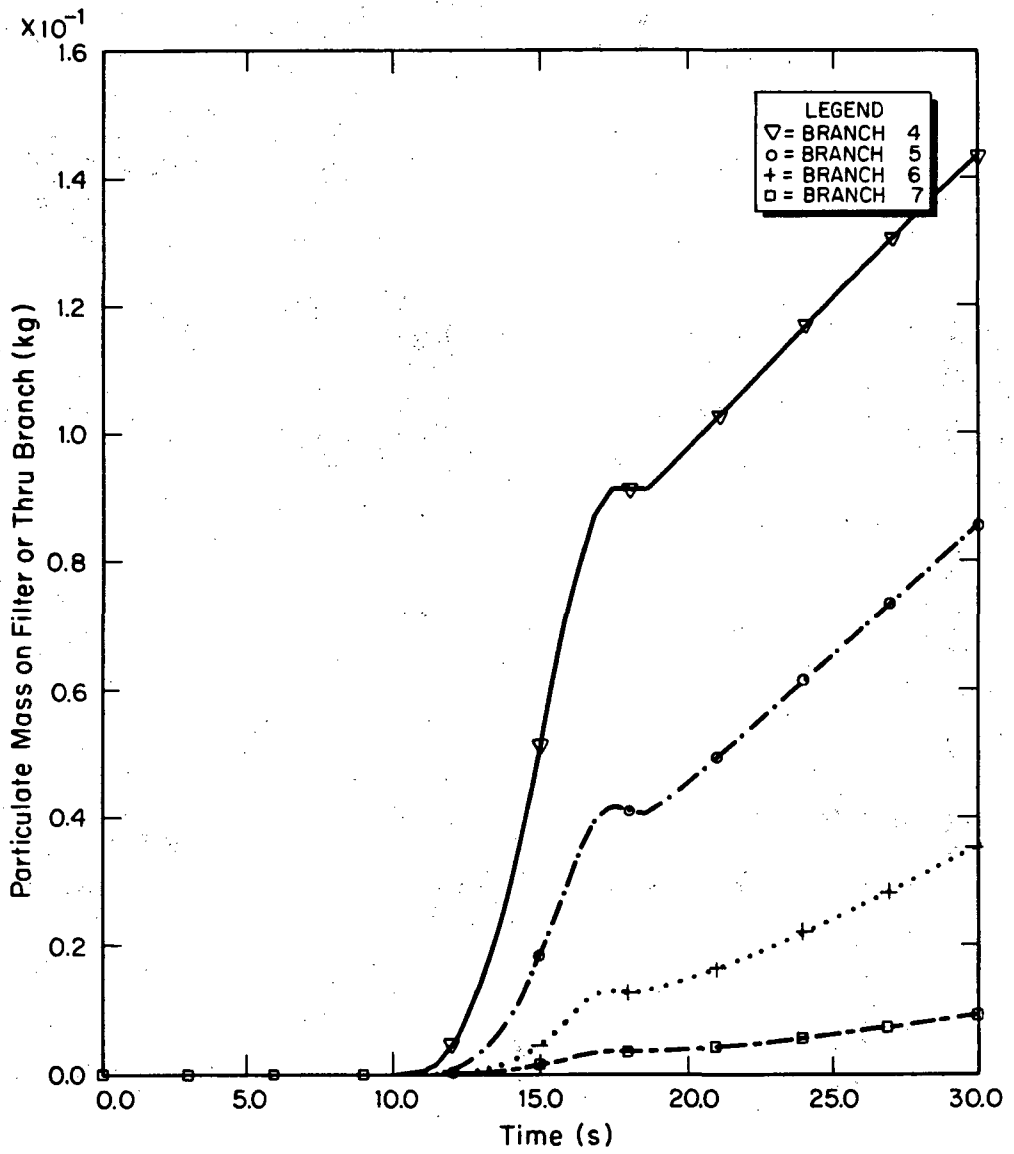

Fig. 31.
Injection: no deposition, T(50).

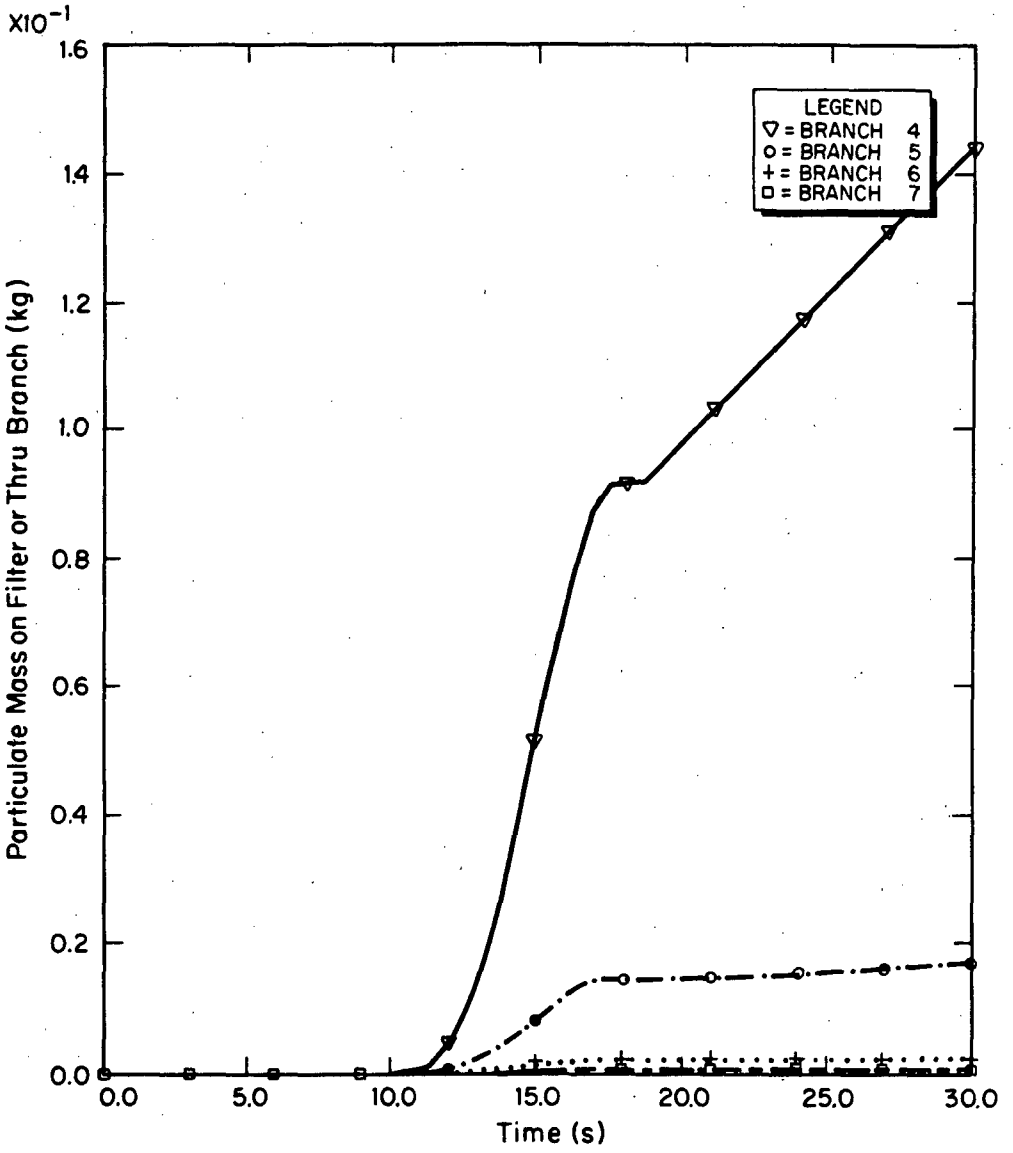

Fig. 32.
Deposition: T(50), D(100).

for the surrounding population. Some uncertainty lies in the estimate of the nuclear facility source term to be used for atmospheric dispersion. In current safety analyses, some conservative assumptions are applied to assess worst cases. Such assumptions are made to assure that the consequences are not underestimated. The current program is intended to improve on our ability to more accurately estimate nuclear facility source terms. Thus, we have undertaken a fuel cycle facility safety analysis program to provide user-oriented tools for making better estimates of accident-induced release or source-term characteristics at a nuclear facility's atmospheric boundaries.[1,2] These tools are intended to be an improvement over current safety analysis review techniques. The scope of the program is limited to only accident-induced material movement within a nuclear facility.

This report is a summary of material transport modeling procedures developed to support a family of accident analysis computer codes. The calculation procedures include transport initiation, convection, interaction, depletion, and filtration. Except for material interaction, these procedures are being used in modular form in TORAC, EXPAC, and FIRAC. This family of codes was developed to provide improved methods of tornado, explosion, and fire accident consequence assessment capability, respectively, for the nuclear industry. The codes were designed to estimate accident-induced gas-dynamic, thermal, and material transport transient phenomena in nuclear fuel cycle facility ventilation systems. However, they are applicable to other facilities as well. Results from sample problems using TORAC have been provided to illustrate current material transport capabilities in a simple system under tornado-induced accident conditions. Some suggestions for future improvements to some of these material transport models also were discussed.

REFERENCES

1. R. W. Andrae, J. W. Bolstad, W. S. Gregory, F. R. Krause, R. A. Martin, P. K. Tang, M. Y. Ballinger, M. K. W. Chan, J. A. Glissmeyer, P. C. Owczarski, J. Mishima, S. L. Sutter, E. L. Compere, H. W. Godbee, and S. Bernstein, "Methods for Nuclear Air Cleaning System Accident Consequence Assessment," Proc. of 17th DOE Nuclear Air Cleaning Conference, Denver, Colorado, August 2-5, 1982 (DOE Symposium Series Conf.-820823, February 1983).

2. "Fuel Cycle Facility Accident Analysis Handbook," Los Alamos National Laboratory report LA-9180-M, NUREG/CR-2508, PNL-4149 in preparation.

3. R. W. Andrae, P. K. Tang, R. A. Martin, and W. S. Gregory, "TORAC Users Manual - A Computer Code for Analysis of Tornado-Induced Flow and Material Transport in Nuclear Facilities," Los Alamos National Laboratory report in preparation.

4. P. K. Tang, R. W. Andrae, J. W. Bolstad, R. A. Martin, and W. S. Gregory, "EXPAC Users Manual - A Computer Code for Analysis of Explosion-Induced Flow and Material Transport in Nuclear Facilities," Los Alamos National Laboratory report in preparation.

5. J. W. Bolstad, R. W. Andrae, W. S. Gregory, F. R. Krause, R. A. Martin, and P. K. Tang, "FIRAC Users Manual - A Computer Code for Analysis of Fire-Induced Flow and Material Transport in Nuclear Facilities," Los Alamos National Laboratory report in preparation.

6. K. H. Duerre, R. W. Andrae, and W. S. Gregory, "TVENT, A Computer Program for Analysis of Tornado-Induced Transients in Ventilation Systems," Los Alamos Scientific Laboratory report LA-7397-M (July 1978).

7. P. K. Tang, "A New Numerical Method for the Transient Gas-Dynamic Code EVENT," Los Alamos National Laboratory report LA-9594-MS (December 1982).

8. D. C. Kaul, Ed., "Adversary Actions in the Nuclear Power Fuel Cycles: Reference Events and Their Consequences, Volume IV., Consequence Assessment Methodology," Science Applications Inc. report SAI-152-123-80-1 (March 1981).

9. S. H. Friedlander, Smoke, Dust and Haze (John Wiley and Sons, New York, 1977).

10. T. T. Mercer, Aerosol Technology in Hazard Evaluation (Academic Press, New York, 1973).

11. R. Dennis, "Handbook on Aerosols," Technical Information Center Energy Research and Development Administration report TID-26608 (1978).

12. N. A. Fuchs, The Mechanics of Aerosols (Pergamon Press Ltd., Oxford, 1964).

13. S. L. Soo, Fluid Dynamics of Multiphase Systems (Blaisdell Publishing Company, Waltham, Massachusetts, 1967).

14. C. N. Davies, Ed., Aerosol Science (Academic Press, New York, 1966).

15. G. M. Hidy and J. R. Brock, The Dynamics of Aerocolloidal Systems (Pergamon Press Ltd., Oxford, 1970).

16. J. D. Stockham and E. G. Fochtman, Eds., Particle Size Analysis (Ann Arbor Science, Ann Arbor, Michigan, 1978).

17. S. L. Sutter, "Accident-Generated Particulate Materials and Their Characteristics--A Review of Background Information," Pacific Northwest Laboratory report PNL-4154, NUREG/CR-2651 (May 1982).

18. J. C. Elder, M. Gonzales, and H. J. Ettinger, "Plutonium Aerosol Size Characteristics," Health Physics 27, 45-53 (1973).

19. H. J. Ettinger, J. C. Elder, and M. Gonzales, "Size Characteristics of Plutonium Aerosols," Los Alamos Scientific Laboratory report LA-DC-72-920 (1972).

20. W. B. Seefeldt, W. J. Mecham, and M. J. Steindler, "Characterization of Particulate Plutonium Released in Fuel Cycle Operations," Argonne National Laboratory report ANL-75-78 (May 1976).

21. E. C. Hyatt, W. D. Moss, and H. F. Schulte, "Particle Size Studies on Uranium Aerosols from Machining and Metallurgy Operations," J Amer. Indus. Hyg. Assoc. 20(2), 99-107 (1959).

22. L. C. Schwendiman, J. Mishima, and G. E. Stegen, "Airborne Plutonium Release Postulated for Serious Accidents in a Generic Recycle Mixed Oxide Fuel Fabrication Plant," Battelle Pacific Northwest Laboratory unpublished draft report (November 1974), Rev. 1.

23. J. M. Selby, "Considerations in the Assessment of the Consequences of Effluents from Mixed Oxide Fuel Fabrication Plants," Battelle Pacific Northwest Laboratory report BNWL-1697 (1975), Rev. 1.

24. J. Mishima and L. C. Schwendiman, "Airborne Release of Plutonium and its Compounds During Overheating Incidents," Battelle Pacific Northwest Laboratory report BNWL-1691 Part 1 (October 1972), pp. 82-87.

25. R. W. Woodard, "Plutonium Particulate Studies on Booster System No. 3 (Building 771) Filter Plenum," DOW Chemical Co. report CRDL 940610-1 (January 1971).

26. B. R. Fish, G. W. Keilholtz, W. S. Snyder, and S. D. Swisher, "Calculation of Doses Due to Accidentally Released Plutonium from an LMFBR," Oak Ridge National Laboratory report ORNL-NSIC-74 (November 1972).

27. O. J. Wick, Ed., Plutonium Handbook (Gordon and Breach Science Publishers, New York, 1967).

28. E. Walker, "A Summary of Parameters Affecting the Release and Transport of Radioactive Material from an Unplanned Accident," Bechtel Inc. report, San Francisco, California (1978).

29. L. C. Schwendiman, "Supporting Information for the Estimation of Plutonium Oxide Leak Rates Through Very Small Apertures," Battelle Pacific Northwest Laboratory report BNWL-2198 (January 1977).

30. J. Mishima and L. C. Schwendiman, "Some Experimental Measurements of Airborne Uranium (Representing Plutonium) in Transportation Accidents," Battelle Pacific Northwest Laboratory report BNWL-1732 (August 1973).

31. R. W. Andrae, R. A. Martin, and W. S. Gregory, "Analysis of Nuclear Facilities for Tornado-Induced Flow and Reentrainment," Los Alamos Scientific Laboratory report LA-7571-MS, NUREG/CR-0521 (January 1979).

32. J. W. Healy, "Surface Contamination: Decision Levels," Los Alamos Scientific Laboratory report LA-4558-MS (September 1971).

33. B. R. Fish, Surface Contamination (Pergamon Press Ltd., Oxford, 1967).

34. R. J. Englemann and G. A. Sehmel, Coordinators, Atmosphere-Surface Exchange of Particulate and Gaseous Pollutants, ERDA Symposium Series Conf.-740921 (1974).

35. J. M. Singer, E. B. Cook, and J. Grumer, "Dispersal of Coal and Rock Dust Deposits," U.S. Bureau of Mines report BM-RI-7642 (1972).

36. J. M. Singer, M. E. Harris, and J. Grumer, "Dust Dispersal by Explosion-Induced Airflow, Entrainment by Air Blast," U.S. Bureau of Mines report BM-RI-8130 (1976).

37. G. A. Sehmel and F. D. Lloyd, "Particle Resuspension Rates," in Atmosphere-Surface Exchange of Particulate and Gaseous Pollutants, R. J. Englemann and G. A. Sehmel, Coordinators, ERDA Symposium Series Conf.-740921 (1974), pp. 846-858.

38. J. R. Travis, "A Model for Predicting the Redistribution of Particulate Contaminants from Soil Surfaces," Los Alamos Scientific Laboratory report LA-6035-MS (August 1975).

39. J. D. Iversen, J. B. Pollack, R. Greeley, and B. R. White, "Saltation Threshold on Mars: The Effect of Interparticle Force, Surface Roughness, and Low Atmospheric Density," ICARUS 29, 381-393 (1976).

40. J. D. Iversen, R. Greeley, and J. B. Pollack, "Windblown Dust on Earth, Mars, and Venus," J. Atom. Sci. 33(12), 2425-2429 (1976).

41. F. M. White, Viscous Fluid Flow (McGraw-Hill Book Company, Inc., New York, 1974).

42. H. Schlichting, Boundary Layer Theory, 4th Ed. (McGraw-Hill Book Company, Inc., New York, 1960).

43. J. D. Iversen, R. Greeley, B. R. White, and J. B. Pollack, "The Effect of Vertical Distortion in the Modeling of Sedimentation Phenomena: Martian Crater Wake Streaks," J. Geophys. Res. 81(26), 4846-4856 (1976).

44. F. R. Krause and W. S. Gregory, "Simulation of Forced-Ventilation Fires," Proc. of 17th DOE Nuclear Air Cleaning Conf., Denver, Colorado, Aug. 2--5, 1982 (DOE Symposium Series Conf.-820823, February 1983), Vol. 2, pp. 1018-1027.

45. S. L. Sutter, J. W. Johnston, J. Mishima, "Aerosols Generated by Free Fall Spills of Powders and Solutions in Static Air," Battelle Pacific Northwest Laboratory report PNL-3786, NUREG/CR-2139 (December 1981).

46. G. B. Wallis, One-Dimensional Two-Phase Flow (McGraw-Hill Book Company, Inc., New York, 1969).

47. F. A. Williams, Combustion Theory (Addison-Wesley Publishing Company, Reading, Massachusetts, 1965).

48. F. Gelbard and J. H. Seinfeld, "Numerical Solution of the Dynamic Equation for Particulate Systems," J. Comput. Phys. 28, 357 (1978).

49. F. Gelbard and J. H. Seinfeld, "The General Dynamic Equation for Aerosols--Theory and Application to Aerosol Formation and Growth," J. Colloid. Interface Sci. 68, 363 (1979).

50. F. Gelbard, "AEROSOL Users Manual," Sandia National Laboratories, Albuquerque, report SAND 80-0403, NUREG/CR-1367 (March 1981).

51. J. A. Gieseke, K. W. Lee, and L. D. Reed, "HAARM-3 Users Manual," Battelle Columbus Laboratories report BMI-NUREG-1991 (January 1978).

52. F. Gelbard, Y. Fambour, and J. H. Seinfeld, "Sectional Representations for Simulating Aerosol Dynamics," J. Colliod. Interface Sci. 76, 541 (1980).

53. F. Gelbard and J. H. Seinfeld, "Simulation of Multicomponent Aerosol Dynamics," J. Colloid. Interface Sci. 78, 485 (1980).

54. S. K. Friedlander and H. F. Johnstone, "Deposition of Suspended Particles from Turbulent Gas Streams," Ind. Engng. Chem. 49, 1151 (1957).

55. B. Y. H. Liu and J. K. Agarwal, "Experimental Observation of Aerosol Deposition in Turbulent Flow," J. Aerosol Sci. 5, 145 (1974).

56. S. K. Beal, "Deposition of Particles in Turbulent Flow on Channel or Pipe Walls," Nucl. Sci. Engng. 40, 1 (1970).

57. C. S. Lin, R. W. Moulton, and G. L. Putnam, "Mass Transfer Between Solid Wall and Fluid Streams," Ind. Engng. Chem. 45, 636 (1953).

58. H. Matsui, Y. Yoshida, M. Murata, and T. Okata, "Measurement of Deposition Fraction of Aerosol Particles in a Horizontal Straight Metal Pipe," J. Nucl. Sci. and Tech. 11, 26 (1974).

59. W. S. Gregory, H. L. Horak, P. R. Smith, C. I. Ricketts, and W. Gill, "Investigation of HEPA Filters Subjected to Tornado Pressure Pulses," Los Alamos Scientific Laboratory report LA-7202-MS (April 1978).

60. H. D'Arcy, Les Fontaines Publiques de la Ville de Dijon (Victor Dalmont, Paris, 1856).

61. J. Kozeny, "Uber Kapillare Leitung des Wassers in Boden," Akad. Wiss. Wien, Math.-Naturw. Klasses, Sitzber (Abt. IIa) 136, 271-306 (1927).

62. P. C. Carman, "Flow through Granular Beds," Transactions of the Institute of Chemical Engineers 15, 150-166 (1937).

63. A. E. Sheidegger, The Physics of Flow Through Porous Media, 3rd Ed. (University of Toronto Press, Toronto, 1972), pp. 146-148.

64. S. P. Burke and W. B. Plummer, "Gas Flow Through Packed Columns," Ind. Engng. Chem. 20, 1196-1200 (1928).

65. S. Ergun, "Fluid Flow through Packed Columns," Chemical Engineering Progress 48, 89-94 (1952).

66. O. Reynolds, Papers on Mechanical and Physical Subjects (Cambridge University Press, Cambridge, Massachusetts, 1900).

67. J. P. Herzig, D. M. LeClerc and P. LeGoff, "Flow of Suspensions through Porous Media - Application to Deep Filtration," Ind. Engng. Chem. 62(5), 8-35 (May 1970).

68. J. Pich, "Theory of Aerosol Filtration," in Aerosol Science, C. N. Davies, Ed. (Academic Press, New York, 1966), pp. 223-285.

69. W. Bergman, H. Hebard, R. Taylor, and B. Lum, "Electrostatic Filters Generated by Electric Fields," Lawrence Livermore National Laboratory report UCRL-81926 (July 1979).

70. C. N. Davies, Air Filtration (Academic Press, New York, 1973).

DISTRIBUTION

	Copies
Nuclear Regulatory Commission, RD, Bethesda, Maryland	273
Technical Information Center, Oak Ridge, Tennessee	2
Los Alamos National Laboratory, Los Alamos, New Mexico	50
	325

☆U.S. GOVERNMENT PRINTING OFFICE: 1983-0-776-026/99